Title

RAP2 mediates mechanoresponses of the Hippo pathway.

Journal

Nature, 560(7720)

ISSN

0028-0836

Authors

Meng, Zhipeng
Qiu, Yunjiang
Lin, Kimberly C
et al.

Publication Date

2018-08-01

DOI

10.1038/s41586-018-0444-0

Peer reviewed

LETTER

https://doi.org/10.1038/s41586-018-0444-0

RAP2 mediates mechanoresponses of the Hippo pathway

Zhipeng Meng[1], Yunjiang Qiu[2,3], Kimberly C. Lin[1], Aditya Kumar[4], Jesse K. Placone[4], Cao Fang[1], Kuei-Chun Wang[4,5], Shicong Lu[1], Margaret Pan[1], Audrey W. Hong[1], Toshiro Moroishi[1,6,7], Min Luo[1,8], Steven W. Plouffe[1], Yarui Diao[2], Zhen Ye[2], Hyun Woo Park[1,9], Xiaoqiong Wang[10], Fa-Xing Yu[11], Shu Chien[4,5], Cun-Yu Wang[12], Bing Ren[2,13], Adam J. Engler[4] & Kun-Liang Guan[1]*

Mammalian cells are surrounded by neighbouring cells and extracellular matrix (ECM), which provide cells with structural support and mechanical cues that influence diverse biological processes[1]. The Hippo pathway effectors YAP (also known as YAP1) and TAZ (also known as WWTR1) are regulated by mechanical cues and mediate cellular responses to ECM stiffness[2,3]. Here we identified the Ras-related GTPase RAP2 as a key intracellular signal transducer that relays ECM rigidity signals to control mechanosensitive cellular activities through YAP and TAZ. RAP2 is activated by low ECM stiffness, and deletion of RAP2 blocks the regulation of YAP and TAZ by stiffness signals and promotes aberrant cell growth. Mechanistically, matrix stiffness acts through phospholipase Cγ1 (PLCγ1) to influence levels of phosphatidylinositol 4,5-bisphosphate and phosphatidic acid, which activates RAP2 through PDZGEF1 and PDZGEF2 (also known as RAPGEF2 and RAPGEF6). At low stiffness, active RAP2 binds to and stimulates MAP4K4, MAP4K6, MAP4K7 and ARHGAP29, resulting in activation of LATS1 and LATS2 and inhibition of YAP and TAZ. RAP2, YAP and TAZ have pivotal roles in mechanoregulated transcription, as deletion of YAP and TAZ abolishes the ECM stiffness-responsive transcriptome. Our findings show that RAP2 is a molecular switch in mechanotransduction, thereby defining a mechanosignalling pathway from ECM stiffness to the nucleus.

YAP and TAZ function as essential effectors of mechanotransduction to regulate cell proliferation and differentiation[3–7]. When cells are shifted from stiff to soft matrices, YAP and TAZ translocate from the nucleus to the cytoplasm, and are thereby inactivated. However, it is unclear how ECM stiffness is signalled to the Hippo pathway. Because small GTPases function as molecular switches in many biological processes[8], we searched for small GTPases that affect localization of YAP and TAZ in cells seeded on soft (1 kPa) or stiff (40 kPa) matrices (Supplementary Information). RAP2A was identified because its overexpression induced cytoplasmic translocation of YAP and TAZ even on a stiff matrix (Fig. 1a). No other GTPases, including the closely related RAP1B, H-RAS, K-RAS, and N-RAS, showed similar activity (Extended Data Fig. 1a).

At high stiffness, both wild-type MCF10A cells and those in which RAP2A, RAP2B and RAP2C were deleted (RAP2-KO MCF10A cells) showed nuclear localization of YAP and TAZ (Fig. 1b, c). At low stiffness, wild-type cells exhibited mainly cytoplasmic YAP and TAZ, whereas RAP2-KO MCF10A cells retained YAP and TAZ in the nucleus (Fig. 1c). Deletion of RAP2 in HEK293A cells also suppressed cytoplasmic translocation of YAP and TAZ induced by low stiffness (Fig. 1d, e, Extended Data Fig. 1b). Expression of the YAP and TAZ target genes *CTGF*, *CYR61*, and *ANKRD1* was repressed by low stiffness in wild-type cells, but not in RAP2-KO cells (Fig. 1f). Similar results were observed in human mesenchymal stem cells (Extended Data Fig. 1c–e), in which RAP2 deletion suppressed differentiation into adipocytes (Extended Data Fig. 1f, g). In luminal breast cancer MCF7 cells, ECM stiffness modulated localization of YAP and TAZ in a RAP2-dependent manner, whereas the basal type MDA-MB-468 cells showed constitutively cytoplasmic localization of YAP and TAZ regardless of stiffness (Extended Data Fig. 1h–l). TWIST1 and β-catenin have been reported to show nuclear–cytoplasmic shuttling in response to physical cues[9,10]. TWIST1, but not β-catenin, displayed nuclear–cytoplasmic translocation in response to ECM stiffness (Extended Data Fig. 2a). However, RAP2 deletion had no obvious effect on TWIST1 localization.

The activity of small GTPases is switched on and off by binding of GTP and GDP, respectively. A RalGDS-RBD pull-down assay showed that low stiffness promotes binding of GTP to RAP2 (Fig. 2a, Extended Data Fig. 2b). Unlike wild-type RAP2A, the GTP-binding-deficient mutant RAP2A(S17N) did not induce cytoplasmic translocation of YAP and TAZ (Extended Data Fig. 2b, c). PDZGEF1 and PDZGEF2 are RAP2 activators[11–13], and the interaction of RAP2 with PDZGEF1 was enhanced by low stiffness (Extended Data Fig. 2d). We generated cells lacking both activators (PDZGEF1/2-dKO cells; Extended Data Fig. 2e, f) and discovered that they were defective in cytoplasmic translocation of YAP and TAZ (Fig. 2b, c) and target gene repression (Extended Data Fig. 2g) in response to low stiffness. Deletion of PDZGEF1 and PDZGEF2 blunted activation of RAP2 by low stiffness (Fig. 2d), and PDZGEF1 overexpression induced cytoplasmic translocation of YAP and TAZ in wild-type but not RAP2-KO cells (Extended Data Fig. 2h, i).

Phosphatidylinositol-4,5-bisphosphate (PtdIns(4,5)P_2) activates RAP2 through PDZGEF1 and PDZGEF2 at the plasma membrane after PtdIns(4,5)P_2 is converted into phosphatidic acid (PA) by phospholipase D1 (PLD1) and PLD2[13]. Using a GFP-tagged PtdIns(4,5)P_2 reporter, we observed that PtdIns(4,5)P_2 was enriched at the plasma membrane at low stiffness (Fig. 2e, Extended Data Fig. 2j). Focal adhesions decrease PtdIns(4,5)P_2 by activating PLCγ1[14,15]. Inhibition of PLCγ1 by U73122 induced PtdIns(4,5)P_2 accumulation (Extended Data Fig. 2k). We hypothesized that ECM stiffness regulates RAP2, YAP and TAZ by modulating focal adhesion and local PtdIns(4,5)P_2 abundance at the plasma membrane. The focal adhesion kinase (FAK) inhibitor PF573228 or the PLCγ1 inhibitor U73122 increased binding of GTP by RAP2 and cytoplasmic translocation of YAP and TAZ (Extended Data

[1]Department of Pharmacology and Moores Cancer Center, University of California San Diego, La Jolla, CA, USA. [2]Ludwig Institute for Cancer Research, La Jolla, CA, USA. [3]Bioinformatics and Systems Biology Graduate Program, University of California San Diego, La Jolla, CA, USA. [4]Department of Bioengineering, University of California San Diego, La Jolla, CA, USA. [5]Institute of Engineering in Medicine, University of California San Diego, La Jolla, CA, USA. [6]Department of Molecular Enzymology, Faculty of Life Sciences, Kumamoto University, Kumamoto, Japan. [7]Center for Metabolic Regulation of Healthy Aging, Faculty of Life Sciences, Kumamoto University, Kumamoto, Japan. [8]State Key Laboratory of Oral Diseases, National Clinical Research Center for Oral Diseases, West China Hospital of Stomatology, Sichuan University, Chengdu, Sichuan, China. [9]Department of Biochemistry, College of Life Science & Biotechnology, Yonsei University, Seoul, South Korea. [10]Robert J. Tomisch Pathology & Laboratory Medicine Institute, Cleveland Clinic, Cleveland, OH, USA. [11]Children's Hospital and Institutes of Biomedical Sciences, Fudan University, Shanghai, China. [12]Division of Oral Biology and Medicine, School of Dentistry, University of California Los Angeles, Los Angeles, CA, USA. [13]Department of Cellular and Molecular Medicine, Institute of Genomic Medicine, University of California San Diego School of Medicine, La Jolla, CA, USA. *e-mail: kuguan@ucsd.edu

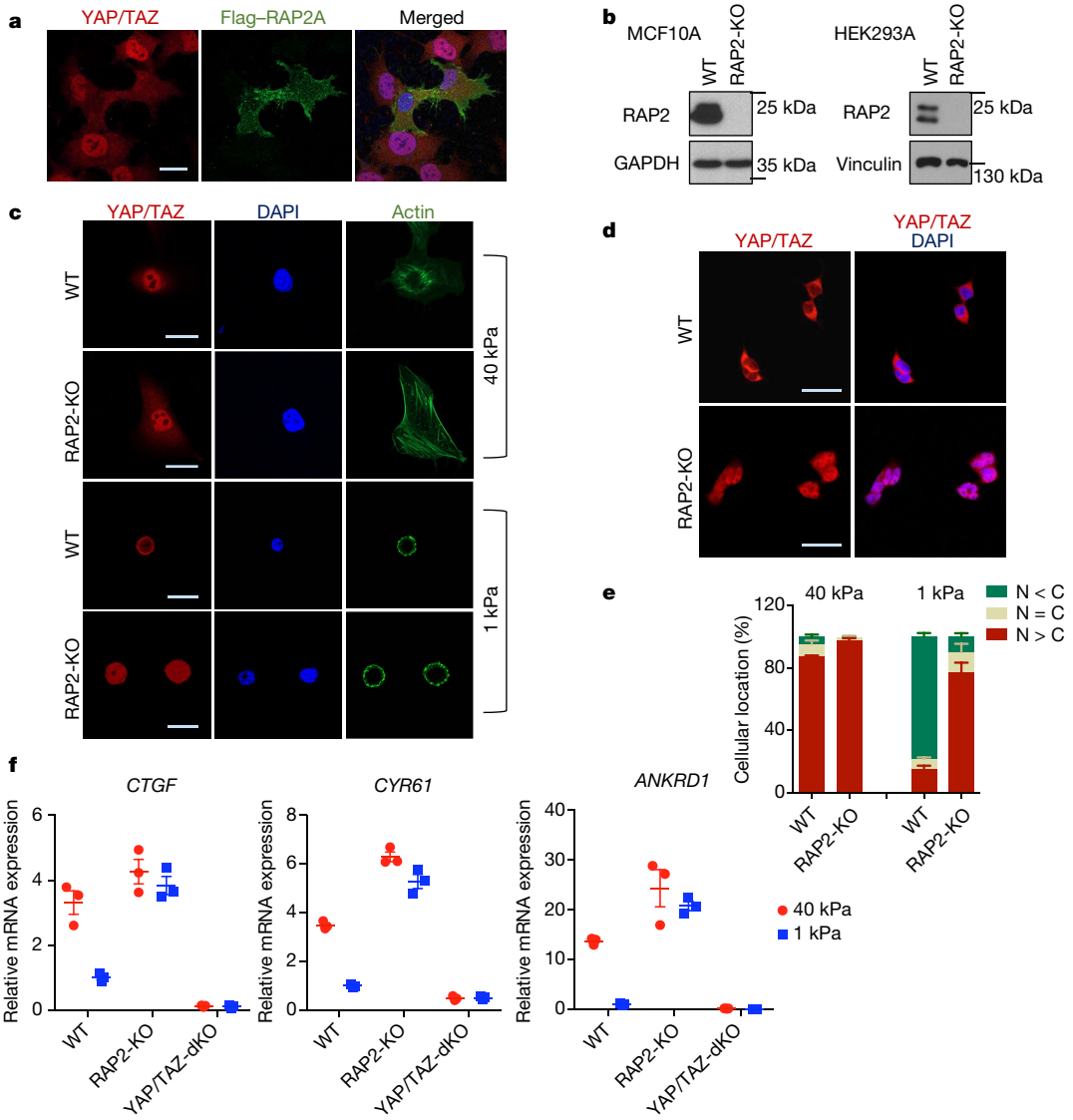

Fig. 1 | RAP2 mediates regulation of YAP and TAZ by ECM stiffness. **a**, Overexpression of Flag–RAP2A induces cytoplasmic translocation of YAP and TAZ in HEK293A cells on a stiff (40 kPa) matrix. Merged, combined signals from YAP and TAZ (red), Flag (green), and DAPI (blue). **b**, Immunoblots showing deletion of RAP2A, RAP2B and RAP2C (RAP2-KO) in MCF10A and HEK293A cells. WT, wild-type. **c**, Immunofluorescence showing that RAP2-KO MCF10A cells, unlike wild-type cells, retain nuclear YAP and TAZ at low stiffness (1 kPa). The experiments in **b** and **c** were repeated independently twice with similar results. **d**, Deletion of RAP2A, RAP2B and RAP2C in HEK293A cells blocks cytoplasmic localization of YAP and TAZ by low stiffness. **e**, Quantification of YAP and TAZ localization, presented as mean + s.e.m., in HEK293A cells. $N < C$, less YAP and TAZ in nucleus than in cytoplasm; $N = C$, similar levels of YAP and TAZ in cytoplasm and nucleus; $N > C$, more YAP and TAZ in nucleus than in cytoplasm. **f**, RAP2 is required for regulation of YAP and TAZ target genes *CTGF*, *CYR61*, and *ANKRD1* by stiffness in HEK293A cells. Data are presented as mean ± s.e.m. For **e** and **f**, $n = 3$ biologically independent samples. Scale bars, 25 μm.

Fig. 3a–c). By contrast, the PLD1 and PLD2 inhibitor BML279 reduced GTP binding by RAP2 and induced the accumulation of YAP and TAZ in the nucleus (Extended Data Fig. 3d–f). The effects of PtdIns(4,5)P_2 on localization of YAP and TAZ were confirmed by experiments involving knockdown of PLCγ1 and combined knockdown of PLD1 and PLD2 (Extended Data Fig. 3g–l).

The nuclear–cytoplasmic shuttling of YAP and TAZ is generally controlled by LATS1- and LATS2-dependent phosphorylation[2]. However, the role of the Hippo kinase cascade in the regulation of YAP and TAZ by mechanotransduction is not clear[4–7]. We found that low ECM stiffness induced phosphorylation of LATS1 and LATS2, and YAP and TAZ, in wild-type cells, and that this phosphorylation was substantially blunted in RAP2-KO cells (Fig. 3a). Furthermore, RAP2 induced YAP phosphorylation in a GTP-binding-dependent manner (Extended Data Fig. 3m). We proposed that RAP2 controls localization of YAP and TAZ via the Hippo pathway. Consistent with this notion, deletion of LATS1 and LATS2 or combined deletion of MST1, MST2 and MAP4Ks abolished regulation of YAP and TAZ by ECM rigidity (Extended Data Fig. 3n, o). Hippo pathway core components were similarly required for RAP2 to induce phosphorylation and cytoplasmic translocation of YAP and TAZ (Extended Data Fig. 4a, b). The role of LATS1 and LATS in this regulation was confirmed in LATS1/2-dKO mouse embryonic fibroblasts, as well as in NF2-KO or MOB1A/MOB1B-dKO HEK293A cells[16,17] (Extended Data Fig. 4c, d).

MAP4K4, TNIK (MAP4K7), and ARHGAP29 are RAP2 effectors[18–20]. Notably, ARHGAP29 is one of the RhoGAPs that are transcriptionally activated by YAP[21,22]. MAP4K4 kinase activity was stimulated by low stiffness in wild-type but not RAP2-KO cells (Extended Data Fig. 4e, f). Moreover, low stiffness induced MAP4K4 phosphorylation, as indicated by reduced mobility, in a RAP2-dependent manner (Extended Data Fig. 4g, h). Deletion of the RAP2-interacting citron domain[19] in MAP4K4 abolished its regulation by RAP2 (Extended Data Fig. 4i, j), and the

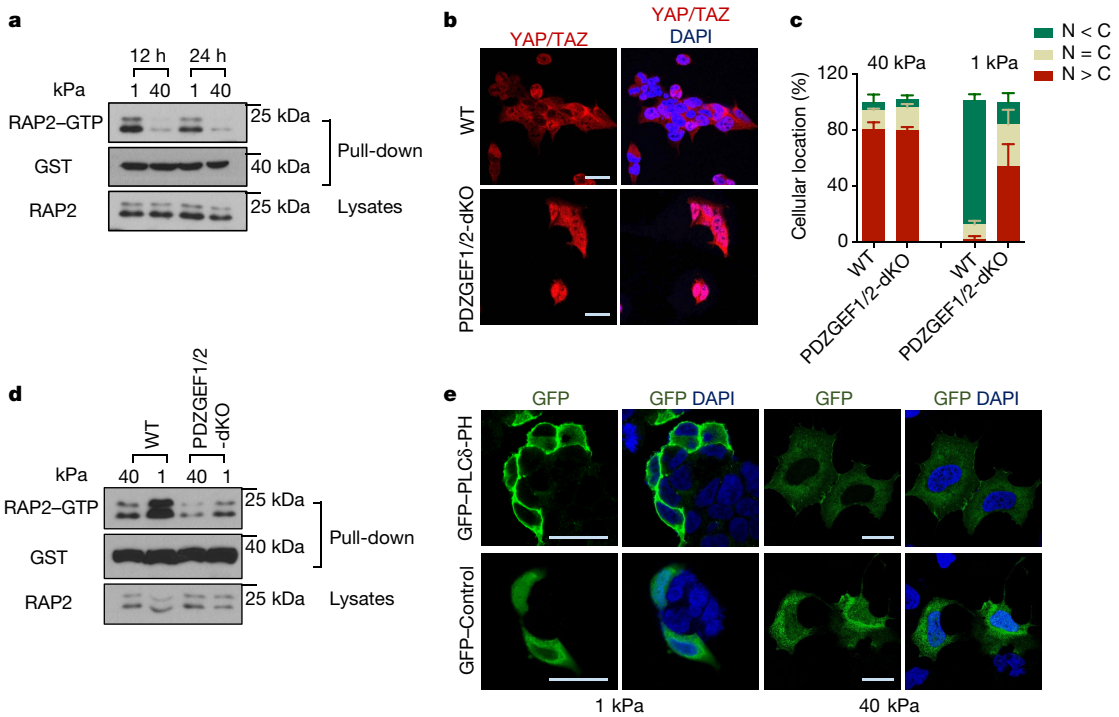

Fig. 2 | ECM stiffness acts via PDZGEF1 and PDZGEF2 to regulate RAP2. a, RAP2 is activated by low stiffness. Pull-down of GTP-bound RAP2 from cells at 1 kPa and 40 kPa using GST–RalGDS-RBD. **b**, Deletion of PDZGEF1 and PDZGEF2 compromises translocation of YAP and TAZ at 1 kPa. **c**, Quantification of YAP and TAZ localization, presented as mean + s.e.m., in **b**. $n = 3$ (40 kPa) or 4 (1 kPa) biologically independent samples. **d**, PDZGEF1 and PDZGEF2 mediate regulation of RAP2 by stiffness. Experiments were similar to **a**. **e**, High stiffness reduces enrichment of PtdIns(4,5)P_2 at the plasma membrane. A GFP-tagged PtdIns(4,5)P_2 reporter PLCδ-PH domain was transfected into cells and detected with anti-GFP antibodies. The experiments in **a**, **d**, **e** were repeated independently twice with similar results. Scale bars, 25 μm.

mutant also failed to rescue the YAP and TAZ translocation defect in cells lacking MST1, MST2 and the MAP4Ks (MST1/2-MAP4K1/2/3/4/6/7-8KO cells) (Fig. 3b). Notably, a recent study showed that the *Drosophila* MAP4K4/6/7 homologue Msn regulates Yki in response to tension[23]. In addition, overexpression of RAP2A led to inactivation of RhoA (Extended Data Fig. 5a), a potent activator for YAP and TAZ[7,16] (Extended Data Fig. 5b–d). This action of RAP2A on RhoA was mediated by ARHGAP29, because YAP phosphorylation induced by ARHGAP29 required its Rho-GAP domain and the Hippo kinase cascade (Fig. 3c, Extended Data Fig. 5e). Deletion of ARHGAP29 compromised inactivation of RhoA by low stiffness (Extended Data Fig. 5f, g). Therefore, RAP2 acts through MAP4K4, MAP4K6, MAP4K7 and ARHGAP29 to inhibit YAP and TAZ. Consistent with this finding, MAP4K4/6/7-ARHGAP29-4KO cells were resistant to RAP2-induced cytoplasmic translocation and phosphorylation of YAP and TAZ (Fig. 3d, Extended Data Fig. 5h), and displayed impaired responses to ECM stiffness (Fig. 3e, Extended Data Fig. 5i). Collectively, our data reveal a signalling axis that links matrix stiffness to regulation of YAP and TAZ as follows: focal adhesion→PLCγ1→PtdIns(4,5)P_2→PA→PDZGEF→RAP2→ARHGAP29 and MAP4K→LATS (Fig. 3f), which works in parallel to the cell spreading–RhoA–cytoskeleton tension-mediated YAP and TAZ translocation mechanism proposed previously[4,7].

RAP2 is activated by cell–cell contact[12], which also presents a mechanical cue to cells and inhibits YAP and TAZ[2,17]. Deletion of RAP2 moderately increased nuclear YAP and TAZ at high confluence (Extended Data Fig. 6a, b). Combined deletion of RAP2 with MST1 and MST2 resulted in stronger nuclear accumulation and gene transactivation of YAP and TAZ (Extended Data Fig. 6a–e). Deletion of RAP2, MST1 and MST2 is required to blunt phosphorylation of LATS and inactivation of YAP and TAZ, suggesting that confluency signalling is complex and additional routes, such as cellular junctions, contribute to activation of LATS1 and LATS2.

Deletion of RAP2 selectively enhanced cell growth only at low stiffness (Extended Data Fig. 7a). To assess the role of RAP2 in tumorigenesis, we performed three assays: acinus formation, anchorage-independent growth, and xenotransplantation. First, we used a 3D-culture system with low stiffness hydrogels to assay the formation of MCF10A acini[9] (Extended Data Fig. 7b); aberrant acinus formation represents irregular cell growth and malignant transformation[9,24]. Wild-type cells formed normal acini whereas RAP2-KO cells generated multi-acinar structures (Fig. 4a, b, Extended Data Fig. 7c), and knockdown of YAP and TAZ significantly reduced the development of aberrant acini. Because MST1 and MST2 mediate some physical signals independent of RAP2 (Extended Data Fig. 6), we generated MCF10A cells lacking RAP2A, RAP2B, RAP2C, MST1 and MST2 (RAP2-MST1/2-KO; Extended Data Fig. 7d). Whereas MST1/2-dKO cells formed relatively normal acini, the RAP2-MST1/2-KO cells formed large acini with invasive behaviours (Extended Data Fig. 7e, f) even at 150 Pa, similar to the stiffness of normal breast tissue (Extended Data Fig. 7g, h). Second, a colony-formation assay in soft agar showed that RAP2-MST1/2-KO cells displayed anchorage-independent growth (Extended Data Fig. 8a). Third, RAP2-MST1/2-KO cells showed substantial xenograft growth in immune-deficient mice, whereas MST1/2-dKO cells did not (Fig. 4c, Extended Data Fig. 8b, c). RAP2-MST1/2-KO xenografts contained abundant MCF10A cells recapitulating the acinus and duct formation of breast tissue, whereas MST1/2-dKO xenografts consisted of mainly host cells with a small number of MCF10A cells (Extended Data Fig. 8d, e). Moreover, the RAP2-MST1/2-KO cells displayed architectural and cytological atypia with signs of malignancy (Extended Data Fig. 8e). Consistently, knockdown of YAP and TAZ suppressed xenograft growth (Fig. 4d, Extended Data Fig. 8f–h). The function of RAP2 in stiffness-regulated growth was confirmed in a xenograft model using H-RAS-V12-expressing MCF10A cells[25,26] (Fig. 4e, f, Extended Data Fig. 8i, j). We used LOX-overexpressing fibroblasts or semisynthetic hyaluronan-derived hydrogels (soft: 0.40 ± 0.03 kPa; stiff: 8.98 ± 0.33 kPa)[27,28] to assess the effect of stiffness on cell growth in xenograft models (Extended Data Fig. 9). Under low stiffness or with control fibroblasts, RAP2-KO cells grew significantly larger xenografts than wild-type cells, whereas the growth advantage of RAP2-KO cells was decreased at high stiffness or in the presence of LOX-overexpressing fibroblasts (Fig. 4g, h, Extended Data Fig. 9).

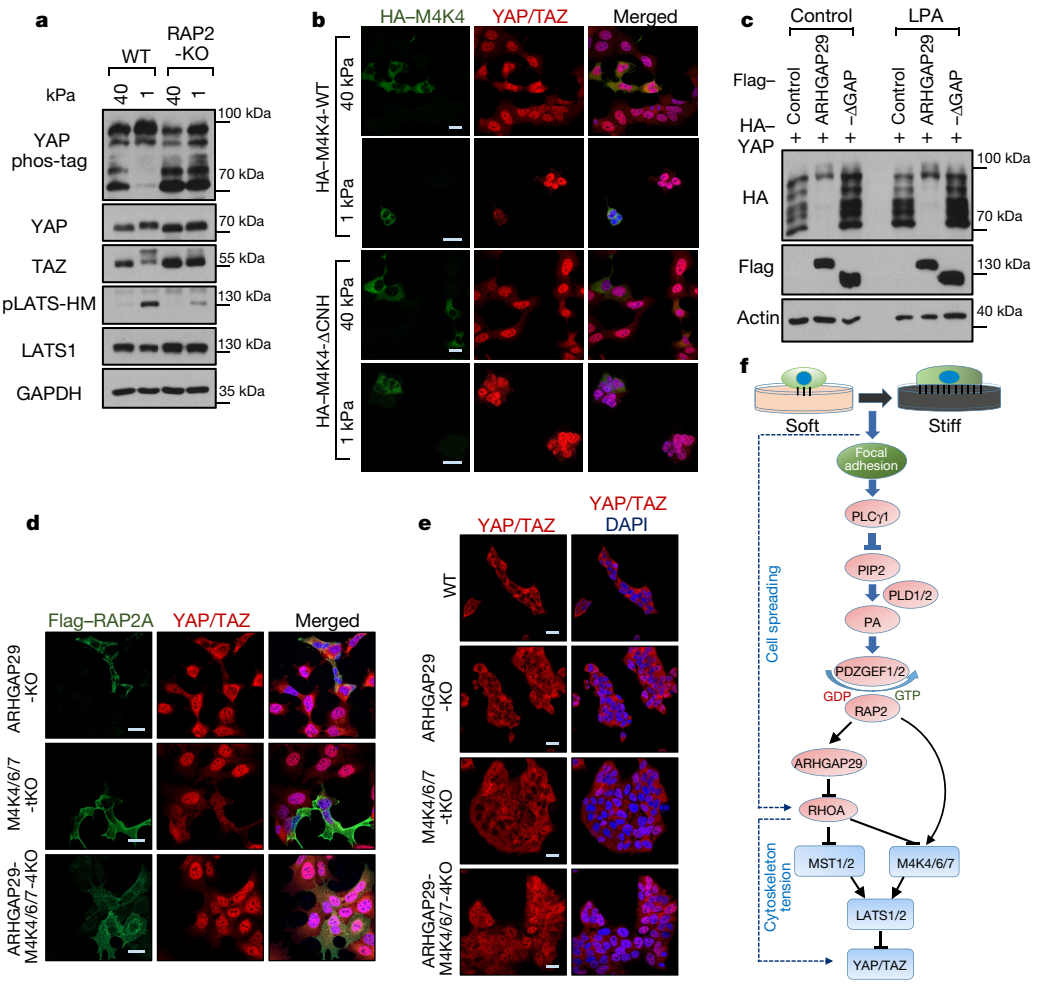

Fig. 3 | RAP2 inhibits YAP and TAZ through MAP4K4, MAP4K6, MAP4K7 and ARHGAP29. a, RAP2 is important for stiffness-regulated phosphorylation of LATS1, LATS2, YAP and TAZ. Phos-tag gel detects YAP phosphorylation by mobility shift. pLATS-HM detects phosphorylation of LATS1 and LATS2 in the hydrophobic motif. **b**, Expression of wild-type MAP4K4 (M4K4-WT), but not the citron domain-deleted mutant (M4K4-ΔCNH), rescued localization of YAP and TAZ in MM-8KO (MST1/2-MAP4K1/2/3/4/6/7-8KO) cells at low stiffness. HA, haemagglutinin. Merged, combined signals from HA–MAP4K4 (green), YAP and TAZ (red), and DAPI (blue). **c**, Overexpression of wild-type ARHGAP29, but not the GAP domain-deleted mutant (ARHGAP29-ΔGAP), induced phosphorylation of YAP. Treatment with lysophosphatidic acid (LPA), which activates RhoA, is indicated. Control, cells without ARHGAP29 overexpression. **d**, Knockout of ARHGAP29 and MAP4K4, MAP4K6 and MAP4K7 blocked RAP2A-induced cytoplasmic localization of YAP and TAZ. Merged, combined signals from Flag–RAP2A (green), YAP and TAZ (red), and DAPI (blue). **e**, Deletion of ARHGAP29 and MAP4K4, MAP4K6 and MAP4K7 blocked cytoplasmic translocation of YAP and TAZ at 1 kPa. For **a**–**e**, the experiments were repeated twice independently with similar results. **f**, A model showing a signalling axis by which stiffness regulates YAP and TAZ. The dotted lines indicate an actin–cytoskeleton-mediated pathway reported previously[7]. Scale bars, 25 μm.

YAP and TAZ are transcriptional co-activators that generate functional output through gene transcription[2]. We performed RNA sequencing (RNA-seq) with RAP2-KO, LATS1/2-dKO, and YAP/TAZ-dKO HEK293A cells to investigate their transcriptional responses to ECM stiffness (Fig. 4i, Extended Data Fig. 10a). In wild-type cells, low stiffness led to downregulation of 814 genes and upregulation of 513 genes. These genes are involved in metabolic processes, such as RNA and macromolecule biosynthesis, and morphogenesis (Supplementary Information). YAP and TAZ are 'gate-keepers' that are responsible for almost all the stiffness-responsive genes, as deletion of YAP and TAZ or LATS1 and LATS2 abolished most of the changes in expression of these genes (Fig. 4i), including *AMOTL2* and *LGR5* (Extended Data Fig. 10b). Consistent with its role in mechanosignalling, RAP2 deletion completely abolished the changes in expression of 40–50% (not including those partially blunted) of stiffness-responsive genes (Fig. 4i).

To assess the interplay of RAP2 and Hippo pathway components in stiffness-dependent gene regulation, we enriched YAP- and TAZ-activating genes that were downregulated by YAP and TAZ knockout at high stiffness and upregulated by LATS1 and LATS2 knockout at low stiffness, and YAP- and TAZ-repressing genes that were conversely regulated (Extended Data Fig. 10c, d). These genes define an ECM–Hippo transcriptome that comprises nearly a third of the genes affected by ECM stiffness (Extended Data Fig. 10e, f). RAP2 deletion completely abolished the responses to ECM in about 50% of ECM–Hippo transcriptome genes (Extended Data Fig. 10g, h), and also partially compromised many genes. The RAP2-regulated ECM–Hippo transcriptome revealed that RAP2 controls genes involved in cell growth and adhesion (for example, *CTGF*, *CYR61*), as well as morphogenesis and development (for example, *KRT8*, *KRT18*, *GDF6*), through the Hippo pathway to respond to ECM stiffness (Fig. 4j, Supplementary Information).

This study shows that RAP2 is an intracellular mechanotransducer that relays extracellular mechanical signals to transcriptional regulation through the Hippo pathway. ECM stiffness acts through RAP2 and its downstream Hippo kinase cascade to modulate a YAP- and TAZ-mediated mechanoresponsive transcriptome. The identification of this signalling axis provides mechanistic insights into how cellular machinery is driven by mechanical stimuli.

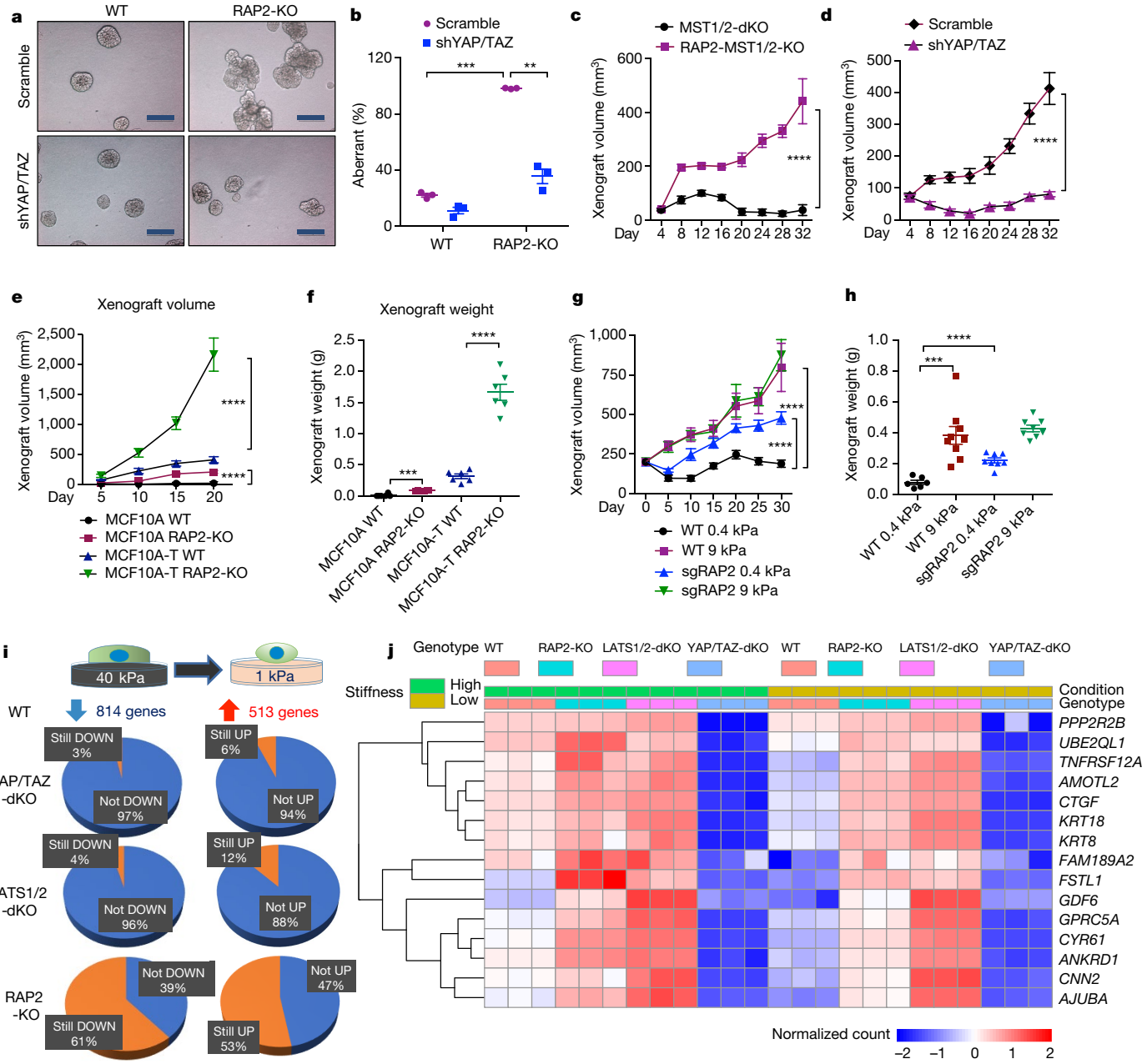

Fig. 4 | RAP2 suppresses cell transformation and regulates the ECM stiffness transcriptome through Hippo and YAP. a, Knockdown of YAP and TAZ (shYAP/TAZ) suppresses the aberrant acinus growth caused by deletion of RAP2A, RAP2B and RAP2C in MCF10A cells. Scale bars, 100 μm. Scramble, control shRNA. **b**, Quantification of aberrant acini from three hydrogels (mean ± s.e.m.). Two-tailed *t*-test: ***RAP2-KO versus wild-type, $P = 0.00022$; **shYAP/TAZ versus scramble, $P = 0.0067$. **c**, MST1/2-dKO and RAP2-MST1/2-KO MCF10A cells were injected subcutaneously into NOD/SCID mice. The tumour volume is shown as mean ± s.e.m. Two-way ANOVA, $n = 6$ biologically independent xenografts, ****$P < 0.0001$. **d**, RAP2-MST1/2-KO MCF10A cells with scramble or shYAP/TAZ were injected into NOD/SCID mice. Tumour volume presented as mean ± s.e.m. Two-way ANOVA, $n = 6$ biologically independent xenografts, ****$P < 0.0001$. **e**, MCF10A and MCF10A-T cells with RAP2 deleted were injected into nude mice. The tumour volume is presented as mean ± s.e.m. Two-way ANOVA, $n = 6$ biologically independent xenografts, ****$P < 0.0001$. **f**, Tumour weights on day 20 from **e** (mean ± s.e.m.). Two-tailed *t*-test: ***$n = 6$, $P = 0.0001$; ****$n = 6$, $P = 0.00007$. **g**, MCF7 cells with lentivirus-mediated CRISPR deletion of RAP2 (sgRAP2) embedded in 200 μl of 0.4 or 9.0 kPa hyaluronan-based gel were injected into nude mice. The xenograft volume is shown as mean ± s.e.m. Two-way ANOVA test, $n = 6$ (wild-type, 0.4 kPa), 8 (sgRAP2, 0.4 or 9.0 kPa), or 9 (wild-type, 9.0 kPa) biologically independent xenografts, ****$P < 0.0001$. **h**, Tumour weights on day 31 from **g** (mean ± s.e.m.). Two-tailed *t*-test: ***$n = 6$ or 9, $P = 0.0006$; ****$n = 6$ or 8, $P = 0.00002$. **i**, Expression of genes downregulated or upregulated by low stiffness in wild-type cells assessed by RNA-seq and compared with YAP/TAZ-dKO, LATS1/2-dKO, and RAP2-KO cells. **j**, Heat map of representative ECM-responsive genes regulated by RAP2 and the Hippo pathway.

Online content

Any methods, additional references, Nature Research reporting summaries, source data, statements of data availability and associated accession codes are available at https://doi.org/10.1038/s41586-018-0444-0.

Received: 24 April 2017; Accepted: 12 July 2018;
Published online: 22 August 2018

1. Humphrey, J. D., Dufresne, E. R. & Schwartz, M. A. Mechanotransduction and extracellular matrix homeostasis. *Nat. Rev. Mol. Cell Biol.* **15**, 802–812 (2014).
2. Meng, Z., Moroishi, T. & Guan, K. L. Mechanisms of Hippo pathway regulation. *Genes Dev.* **30**, 1–17 (2016).
3. Halder, G., Dupont, S. & Piccolo, S. Transduction of mechanical and cytoskeletal cues by YAP and TAZ. *Nat. Rev. Mol. Cell Biol.* **13**, 591–600 (2012).
4. Aragona, M. et al. A mechanical checkpoint controls multicellular growth through YAP/TAZ regulation by actin-processing factors. *Cell* **154**, 1047–1059 (2013).

5. Codelia, V. A., Sun, G. & Irvine, K. D. Regulation of YAP by mechanical strain through Jnk and Hippo signaling. *Curr. Biol.* **24**, 2012–2017 (2014).
6. Wada, K., Itoga, K., Okano, T., Yonemura, S. & Sasaki, H. Hippo pathway regulation by cell morphology and stress fibers. *Development* **138**, 3907–3914 (2011).
7. Dupont, S. et al. Role of YAP/TAZ in mechanotransduction. *Nature* **474**, 179–183 (2011).
8. Cherfils, J. & Zeghouf, M. Regulation of small GTPases by GEFs, GAPs, and GDIs. *Physiol. Rev.* **93**, 269–309 (2013).
9. Wei, S. C. et al. Matrix stiffness drives epithelial–mesenchymal transition and tumour metastasis through a TWIST1–G3BP2 mechanotransduction pathway. *Nat. Cell Biol.* **17**, 678–688 (2015).
10. Benham-Pyle, B. W., Pruitt, B. L. & Nelson, W. J. Mechanical strain induces E-cadherin-dependent Yap1 and β-catenin activation to drive cell cycle entry. *Science* **348**, 1024–1027 (2015).
11. de Rooij, J. et al. PDZ-GEF1, a guanine nucleotide exchange factor specific for Rap1 and Rap2. *J. Biol. Chem.* **274**, 38125–38130 (1999).
12. Monteiro, A. C. et al. Trans-dimerization of JAM-A regulates Rap2 and is mediated by a domain that is distinct from the *cis*-dimerization interface. *Mol. Biol. Cell* **25**, 1574–1585 (2014).
13. Gloerich, M. et al. Rap2A links intestinal cell polarity to brush border formation. *Nat. Cell Biol.* **14**, 793–801 (2012).
14. Carloni, V., Romanelli, R. G., Pinzani, M., Laffi, G. & Gentilini, P. Focal adhesion kinase and phospholipase C gamma involvement in adhesion and migration of human hepatic stellate cells. *Gastroenterology* **112**, 522–531 (1997).
15. Zhang, X. et al. Focal adhesion kinase promotes phospholipase C-γ1 activity. *Proc. Natl Acad. Sci. USA* **96**, 9021–9026 (1999).
16. Plouffe, S. W. et al. Characterization of Hippo pathway components by gene inactivation. *Mol. Cell* **64**, 993–1008 (2016).
17. Meng, Z. et al. MAP4K family kinases act in parallel to MST1/2 to activate LATS1/2 in the Hippo pathway. *Nat. Commun.* **6**, 8357 (2015).
18. Myagmar, B. E. et al. PARG1, a protein-tyrosine phosphatase-associated RhoGAP, as a putative Rap2 effector. *Biochem. Biophys. Res. Commun.* **329**, 1046–1052 (2005).
19. Machida, N. et al. Mitogen-activated protein kinase kinase kinase kinase 4 as a putative effector of Rap2 to activate the c-Jun N-terminal kinase. *J. Biol. Chem.* **279**, 15711–15714 (2004).
20. Taira, K. et al. The Traf2- and Nck-interacting kinase as a putative effector of Rap2 to regulate actin cytoskeleton. *J. Biol. Chem.* **279**, 49488–49496 (2004).
21. Qiao, Y. et al. YAP regulates actin dynamics through ARHGAP29 and promotes metastasis. *Cell Reports* **19**, 1495–1502 (2017).
22. Porazinski, S. et al. YAP is essential for tissue tension to ensure vertebrate 3D body shape. *Nature* **521**, 217–221 (2015).
23. Li, Q. et al. Ingestion of food particles regulates the mechanosensing misshapen–yorkie pathway in *Drosophila* intestinal growth. *Dev. Cell* **45**, 433–449 (2018).
24. Debnath, J., Muthuswamy, S. K. & Brugge, J. S. Morphogenesis and oncogenesis of MCF-10A mammary epithelial acini grown in three-dimensional basement membrane cultures. *Methods* **30**, 256–268 (2003).
25. Yoh, K. E. et al. Repression of p63 and induction of EMT by mutant Ras in mammary epithelial cells. *Proc. Natl Acad. Sci. USA* **113**, E6107–E6116 (2016).
26. Dawson, P. J., Wolman, S. R., Tait, L., Heppner, G. H. & Miller, F. R. MCF10AT: a model for the evolution of cancer from proliferative breast disease. *Am. J. Pathol.* **148**, 313–319 (1996).
27. Serban, M. A., Scott, A. & Prestwich, G. D. Use of hyaluronan-derived hydrogels for three-dimensional cell culture and tumor xenografts. *Curr. Protoc. Cell Biol.* Ch. 10, Unit 10 14 (2008).
28. Levental, K. R. et al. Matrix crosslinking forces tumor progression by enhancing integrin signaling. *Cell* **139**, 891–906 (2009).

Acknowledgements K.C.L., A.W.H., and S.W.P. are supported by the T32 GM007752 training grant, A.K. by T32AR060712, and J.K.P. by F32HL126406. K.-L.G. is supported by grants from the NIH (CA196878, CA217642, GM51586, DEO15964) as is A.J.E. (R21CA217735, R01CA206880). A.J.E. is also supported by NSF grant 1463689, and A.K. is supported by the NSF graduate research fellowship program and an ARCS/ Roche Foundation Scholar Award in Life Science. H.W.P. is supported by KHIDI grant HI17C1560.

Reviewer information *Nature* thanks M. Sudol, V. Weaver and the other anonymous reviewer(s) for their contribution to the peer review of this work.

Author contributions Z.M. and K.-L.G. conceived the project and wrote the manuscript. Z.M., K.C.L., C.F., S.L., M.P., T.M. and M.L. performed in vitro cell assays, CRISPR knockout, quantitative real-time PCR, immunofluorescence, and xenograft studies. A.K., J.K.P., K.-C.W., A.W.H., S.C. and A.J.E. assisted in manufacturing hydrogels and with immunofluorescence experiments. S.W.P. and H.W.P. provided knockout cell lines. Y.Q., Y.D., Z.Y. and B.R. performed the next-generation sequencing and bioinformatics analyses. X.W. performed the pathological analyses. F.-X.Y., C.-Y.W., B.R. and A.J.E. provided technical support.

Competing interests K.-L.G. is a co-founder of Vivace Therapeutics. The other authors declare no competing interests.

Additional information

Extended data is available for this paper at https://doi.org/10.1038/s41586-018-0444-0.
Supplementary information is available for this paper at https://doi.org/10.1038/s41586-018-0444-0.
Reprints and permissions information is available at http://www.nature.com/reprints.
Correspondence and requests for materials should be addressed to K.-L.G.

METHODS

Cell culture. HEK293A cells were maintained in DMEM containing 10% fetal bovine serum. MCF10A cells were from ATCC and maintained as previously described[24]. The pre-malignant derivative of MCF10A cells, MCF10A-T, were generated by infecting MCF10A cells with a lentiviral vector expressing a constitutively active H-Ras mutant (G12V) as previously described[25,26]. Adipocyte-derived mesenchymal stem cells (MSCs) were cultured in HMSC growth medium from Cell Applications Inc., and were differentiated into adipocytes and stained according to a modified protocol[29]. MCF7 and MDA-MB-468 cells were from ATCC and maintained in DMEM/F12 with 10% FBS. Insulin (0.01 mg/ml) was used for maintaining MCF7 cells. The cell lines were tested to be free of mycoplasma contamination and not experimentally authenticated.

Plasmids. Flag-pLJM1-RAP2A and pRK5-HA-GST-RAP2A plasmids were provided by D. M. Sabatini (Addgene 19311 and 14952). PDZGEF1 and ARHGAP29 coding sequences were subcloned from cDNA clones BC117321 and BC093741 (Transomics Technology), respectively. GFP-C1-PLCdelta-PH was a gift from T. Meyer (Addgene 21179).

The CRISPR–Cas9 system was used to delete genes in HEK293A, MCF10A, MSC, MCF7 and MDA-MB-468 cells. The plasmids px459 v2 and lentiCRISPR v2 were provided by F. Zhang (Addgene 62988 and 52961).

The single-guide RNA (sgRNA) sequences targeting individual genes were as following: *RAP2A* #1: GATGCGCGAGTACAAAGTGG; *RAP2A* #2: GTATTTC TCG ATG AAGGTGC; *RAP2B* #1: CATGAGAGAGTACAAAGTGG; *RAP2B* #2: GGAGCCCGTCACGAACTGCA; *RAP2C* #1: GGTGAAGGTGAGACTCATGA; *RAP2C* #2: AGTGACAAACTGCACAGTAA; *PDZGEF1* (also known as *RAPGEF2*) #1: CCCATAACTCCATGGTTAGC; *PDZGEF1* (also known as *RAPGEF2*) #2: CC AGCTAACCATGGAGTTAT; *PDZGEF2* (also known as *RAPGEF6*) #1: TCAA CGCCTGCCTAGCGCCA; *PDZGEF2* (also known as *RAPGEF6*) #2: GCCACCCG AGCGGACTCCCG; *ARHGAP29* #1: CTCTACTTACATATT TCCAA; *ARHGAP29* #2: AGTTATTCATATACGTCTAG.

RAP2-GTP and RhoA-GTP binding assay. The GST-RalGDS-RBD-expressing BL21 strain was provided by R. Firtel, and the GST-Rhotekin-RBD-expressing BL21 strain was a gift from J. Heller Brown at the University of California, San Diego. The recombinant proteins were purified and stored bound to glutathione-agarose beads. The binding of RAP2-GTP and RhoA-GTP from cell lysates to RalGDS-RBD-agarose and Rhotekin-RBD-agarose beads, respectively, was performed in a buffer containing 50 mM Tris-HCl pH 7.5, 150 mM NaCl, 25 mM $MgCl_2$, 10% glycerol, 0.5% NP-40 substitute and 1 mM DTT.

Cell culture with 2D or 3D polyacrylamide-based hydrogels. 2D culture on hydrogels of high (40.40 ± 2.39 kPa) or low (1.00 ± 0.31 kPa) stiffness was as described elsewhere[30]. In brief, 10 μg/ml human placenta fibronectin or 25–50 ug/ml rat tail collagen I were used to coat the sulfo-sanpah-activated hydrogels according to the preferences of the cell lines. 3D culture followed a protocol with the modification that the Matrigel base was replaced with fibronectin-coated hydrogels[9,24].

Staining and microscopy. For immunofluorescence, cells were fixed in 4% formaldehyde/PBS for 10 min and then were treated with 0.1% Triton X-100 or saponin (only for staining PIP2 GFP reporter) for 15 min. After blocking, the cells were stained with corresponding antibodies. Most images were captured with a Nikon Eclipse Ti confocal microscope and then were exported from NIS elements imaging software. Images in Fig. 2d and Extended Data Fig. 4c, d were taken with an Olympus FV1000 confocal microscope, and Image J was used to merge the signals from channels. For immunohistochemistry, xenografts were subjected to heat-induced antigen retrieval using 10 mM sodium citrate buffer followed by 3% H_2O_2 for 30 min to quench endogenous peroxidase activity. Sections were incubated overnight at 4 °C with YAP/TAZ antibody and detected using Vectastain elite ABC kit and DAB Peroxidase Substrate kit (Vector Laboratories) according to the manufacturer's protocol.

Preparation of semi-synthetic hyaluronan-derived hydrogels. Under aseptic conditions, Glycosil (ESI Bio, GS222), Gelin-S, (ESI Bio, GS231), and Extralink (ESI Bio, GS3006) were dissolved in degassed water (ESI Bio, GS240) according to the manufacturer's directions. To make soft hydrogels, stock concentrations of 10 mg/ml Glycosil, 10 mg/ml Gelin-S, and 5 mg/ml Extralink were made per manufacturer's directions. To make stiff hydrogels, concentrated stocks of Glycosil and Extralink were prepared by solubilization in reduced volumes to make 2× Glycosil and 5× Extralink. Prior to use, aliquots were taken from each vial to make solutions at 1:5 ratios of Extralink: (Glycosil + Gelin-S) and 5× Extralink: (2× Glycosil + Gelin-S) for soft and stiff hydrogels, respectively. For all conditions, the amount of Gelin-S was kept constant to ensure the same number of gelatin-based cell binding sites.

In order to perform atomic force microscopy, the Glycosil and Gelin-S components were mixed thoroughly and then the Extralink was added to initiate gelation. Subsequently, 50 μl of the mixture was added drop-wise to DCMS-treated glass slides and a methacrylated coverslip was placed on top. Each sample was prepared in triplicate. The slides were then incubated at 37 °C until complete gelation. For the samples tested, this occurred within 30–40 min of incubation at 37 °C. Upon gelation, hydrogel stiffness was measured by AFM. Hydrogels were then placed in PBS containing 1% antibiotic/antimycotic at 37 °C and the stiffness was measured 1, 24, and 48 h after mixing.

AFM measurement procedure. AFM was performed to measure hydrogel stiffness as previously described[31]. In brief, indentations were made using a pyrex-nitride probe with a pyramid tip (spring constant ~0.04 N/m, 35° half-angle opening, NanoAndMore USA Corporation, PNP-TR) connected to a MFP-3D Bio Atomic Force Microscope (Oxford Instruments) mounted on a Ti-U fluorescence inverted microscope (Nikon Instruments). Probes were calibrated using the Igor 6.34A software (WaveMetrics). Samples were then loaded on the AFM, submersed in PBS, and indented at a velocity of 2 μm/s with a trigger force of 2 nN. About 20 force measurements were performed over a 90 μm × 90 μm region per gel. Measurements were made each day for three separate gels per condition. Elastic modulus was calculated based on a Hertz-based fit using a built-in code written in Igor 6.34A software.

Animal studies. Female NOD/SCID mice (8–9 weeks old) were purchased from Jackson Laboratory, and 8–9-week-old female nude mice were provided by the animal care program at University of California, San Diego. The mice were hosted in a special pathogen-free room under standard 12:12-h light:dark cycle, fed with standard rodent chow and water ad libitum, and randomized before experiments. The sample size choice was not pre-determined for each experiment. When comparing RAP2-MST1/2-KO MCF10A cells and MST1/2-dKO MCF10A cells, a total of 5×10^6 MCF10A cells in 50% high concentration Matrigel (BD Bioscience) dissolved in PBS were subcutaneously inoculated into a NOD/SCID mouse. When comparing RAP2-KO MCF10A and MCF10A-T cells with wild-type MCF10A and MCF10A-T cells, 5×10^6 cells in 50% Matrigel were injected into nude mice subcutaneously. When comparing RAP2-KO with wild-type MCF7 cells, 2×10^6 MCF7 cells and 4×10^5 LOX-expressing or control NIH3T3 cells in 50% Matrigel/PBS were co-injected subcutaneously into nude mice. For the semi-synthetic hyaluronan-derived hydrogels, 2×10^6 MCF7 cells in 20 μl PBS suspension were embedded into 200 μl of soft and stiff formulations as described in the preparation of hydrogels. After brief gelation (5 min) at room temperature, the cell-laden hydrogels were subcutaneously injected into nude mice. The investigators were blinded to group allocations during data collection and analyses. All procedures followed the NIH guidelines for the care and use of laboratory animals and the IACUC at the University of California, San Diego approved the experiments. For subcutaneous tumour growth, the maximum single tumour cannot exceed 2 cm in diameter in mice according to the guidelines provided by the animal care program at University of California, San Diego, and no experiments in this study generated tumour burden over this limit.

RNA interference. The lentiviral vectors pLKO.1-hygromycin (Addgene 24150) and pLKO.1-Blasticidin (Addgene 26655) were used to clone the following sense sequences to knock down human YAP or TAZ: negative control: CCTA AGGTTAAGTCGCCCTCG (cloned into pLKO.1-hygromycin and pLKO.1-blasticidin); YAP#1: GCCACCAAGCTAGATAAAGAA (pLKO.1-hygromycin); YAP#2: GACATCTTCTGGTCAGAGATA (pLKO.1-hygromycin); TAZ#1: GCGTTCTTGTGACAGATTATA (pLKO.1-blasticidin); TAZ#2: GCTCATGA GTATGCCCAATGC (pLKO.1-blasticidin). The resulting plasmids were used to package lentiviruses and the target cells were infected with an MOI of 0.5.

Duplex siRNAs targeting PLCγ1 and PLD1/2 were purchased from Integrated DNA Technologies, Inc. and transfected into cells with RNAiMAX (ThermoFisher Scientific). The sequences are as follows:

PLCγ1 #1 sense strand 5′-rGrArCrCrUrCrArUrCrArGrCrUrArCrUrArUrGrAr GrArAAC-3′; anti-sense strand 5′-rGrUrUrUrCrUrCrArUrArGrUrArGrCrUrGr ArUrGrArGrGrUrCrArA-3′.

PLCγ1 #2 sense strand 5′-rGrGrCrArArGrArArGrUrUrCrCrUrUrCrAr GrUrArCrArATC-3′; anti-sense strand 5′-rGrArUrUrGrUrArCrUrGrArArGr GrArArCrUrUrCrUrUrGrCrCrUrU-3′. PLD1 #1 sense strand 5′-rGrUrGrGrArUr ArArArUrUrArCrArUrArUrCrArUrUrCrUGT-3′; antisense strand 5′-rArCrArGr ArArUrGrArUrArUrGrUrArArUrUrUrArUrCrCrArCrUrG-3′.

PLD1 #2 sense strand 5′-rArCrUrGrGrArArGrArUrUrArCrUrUrGrArCrArAr ArGrATA-3′; anti-sense strand 5′-rUrArUrCrUrUrUrGrUrCrArArGrUrArArUr CrUrUrCrCrArGrUrUrG-3′.

PLD2 #1 sense strand 5′-rArArCrCrArArGrArArGrArArArUrArCrCrGrUr CrArUrUTT-3′; anti-sense strand 5′-rArArArArUrGrArCrGrGrUrArUrUrUrCr UrUrCrUrUrGrGrUrUrGrU-3′.

PLD2 #2 sense strand 5′-rCrUrCrUrArCrArUrUrGrArGrArArUrCrArGrUrUr CrUrUCA-3′; anti-sense strand 5′-rUrGrArArGrArArCrUrGrArUrUrCrUrCrAr ArUrGrUrArGrArGrGrA-3′.

Quantitative real-time PCR. Total RNAs were extracted with a kit from Qiagen. Reverse transcription was performed with iScript from Bio-Rad. Real-time PCR was performed with the Applied Biosystems 7300 with primers targeting *CTGF*,

CYR61, and *ANKRD1*: *CTGF*-Forward: 5′-CCAATGACAACGCCTCCTG-3′, *CTGF*-Reverse: 5′-TGGTGCAGCCAGAAAGCTC-3′; *CYR61*-Forward: 5′-AGCCTCGCATCCTATACAACC-3′, *CYR61*-Reverse: 5′-TTCTTTCACAAGGCGGCACTC-3′; *ANKRD1*-Forward: 5′-GTGTAGCACCAGATCCATCG-3′, *ANKRD1*-Reverse: 5′-CGGTGAGACTGAACCGCTAT-3′. The gene expression was normalized to *GAPDH*: Forward: 5′-TGCACCACCAACTGCTTAGC-3′; Reverse: 5′-GGCATGGACTGTGGTCATGAG-3′.

RNA sequencing and bioinformatics analysis. Total RNAs were extracted using TRIzol (Thermo Fisher Scientific) from HEK293A cells seeded on high and low stiffness fibronectin-coated hydrogels. Three replicates for each sample were generated and analysed. The resulting RNA was then used to prepare libraries using Illumina TruSeq Stranded mRNA Library Prep Kit Set A (Illumina, RS- 122-2101) or Set B (Illumina, RS-122-2102). The libraries were sequenced using Illumina HiSeq 4000 (single-end 50-bp reads). Reads were aligned to the hg19 reference genome using STAR[32]. Only uniquely mapped reads were kept for further analysis. Number of reads for each gene were counted using htseq-count[33] according to Gencode human annotation release 24. DeSeq2[34] was used to identify differential expressed genes with default parameters. Genes with adjusted P value <0.1 were considered to be differentially expressed. GO and KEGG enrichment analysis of differential expressed genes was performed using DAVID[35].

Statistical analysis. Microsoft Excel was used for t-tests, and Graphpad Prism v6 was used for two-way ANOVA tests. When P is smaller than 0.0001, Graphpad Prism v6 does not provide a precise P value and instead only shows a range of $P < 0.0001$.

Data availability. Source Data for Figs. 1, 2, 4 and Extended Data Figs. 1–3, 5, 7–9 can be found in the online version of the paper. For uncropped images of western blot data, see Supplementary Fig. 1. The RNA sequencing data are available in GEO Data Sets with the accession number GSE98547. All other data that support the findings of this study are available upon request from the corresponding author.

29. Wen, J. H. et al. Interplay of matrix stiffness and protein tethering in stem cell differentiation. *Nat. Mater.* **13**, 979–987 (2014).
30. Tse, J. R. & Engler, A. J. Preparation of hydrogel substrates with tunable mechanical properties. *Curr. Protoc. Cell Biol.* Ch. 10, Unit 10 16 (2010).
31. Kaushik, G., Fuhrmann, A., Cammarato, A. & Engler, A. J. In situ mechanical analysis of myofibrillar perturbation and aging on soft, bilayered *Drosophila* myocardium. *Biophys. J.* **101**, 2629–2637 (2011).
32. Dobin, A. et al. STAR: ultrafast universal RNA-seq aligner. *Bioinformatics* **29**, 15–21 (2013).
33. Anders, S., Pyl, P. T. & Huber, W. HTSeq—a Python framework to work with high-throughput sequencing data. *Bioinformatics* **31**, 166–169 (2015).
34. Love, M. I., Huber, W. & Anders, S. Moderated estimation of fold change and dispersion for RNA-seq data with DESeq2. *Genome Biol.* **15**, 550 (2014).
35. Dennis, G. Jr et al. DAVID: Database for annotation, visualization, and integrated discovery. *Genome Biol.* **4**, 3 (2003).

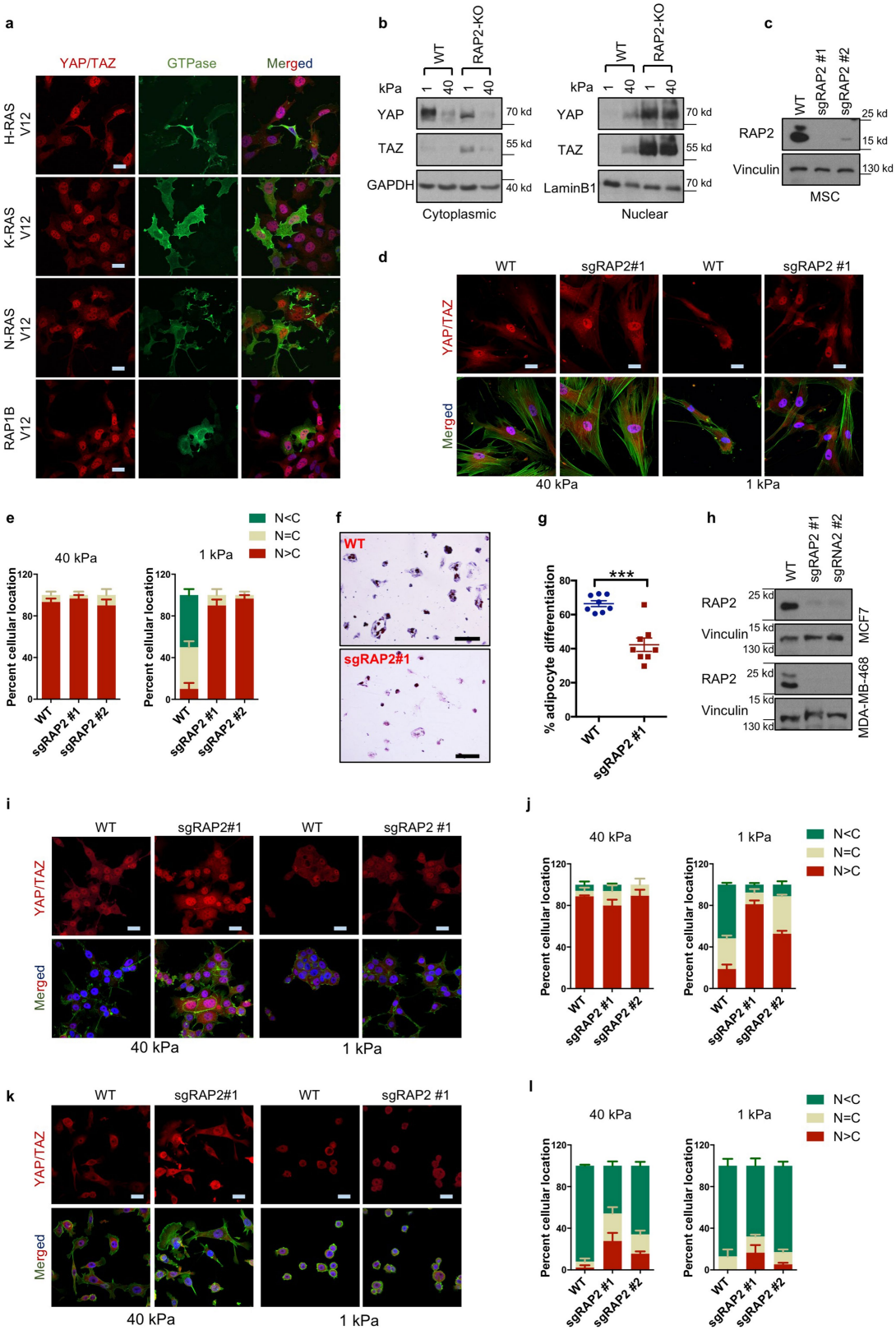

Extended Data Fig. 1 | See next page for caption.

Extended Data Fig. 1 | RAP2 is involved in regulation of YAP and TAZ by matrix stiffness. a, Localization of YAP and TAZ is not significantly affected by overexpression of H-RAS, K-RAS, N-RAS, or RAP1B. HEK293A cells were cultured on high-stiffness hydrogels. Overexpression of HA-tagged H-RAS, K-RAS, N-RAS, and Flag-tagged RAP1B are indicated. Merged, combined signals of YAP and TAZ (red), transfected small GTPases (green), and DAPI (blue, staining for DNA). Scale bars, 25 μm. The images are representative of two independent experiments with similar results. **b**, Subcellular fractionation of wild-type and RAP2-KO HEK293A cells at low or high stiffness. The images are representative of two independent experiments with similar results. **c**, CRISPR-mediated deletion of RAP2A, RAP2B and RAP2C in adipocyte-derived MSCs by lentiviral transduction. sgRNAs targeting RAP2A, RAP2B, and RAP2C (sgRAP2) were individually cloned into lentiCRISPR v2 (Addgene #52961) plasmids. sgRAP2 #1 and #2 were two sets of three sgRNAs targeting RAP2A, RAP2B, and RAP2C with unique sequences for each RAP2 isoform. Adipocyte-derived MSCs were infected with the sgRAP2 lentiviruses with an MOI of 10 and selected by puromycin. After puromycin selection, the pooled cells were examined for RAP2 protein expression. The images are representative of two independent experiments with similar results. **d**, RAP2 is required for the low stiffness-induced cytoplasmic localization of YAP and TAZ in MSCs. MSCs with CRISPR-mediated deletion of RAP2A, RAP2B and RAP2C were seeded onto 40 kPa and 1 kPa collagen-coated hydrogels, cultured for 24 h, and then stained for YAP and TAZ. The results are representative of three biologically independent samples showing similar results. Merged, combined signals of YAP and TAZ (red), F-actin (green), and DAPI (blue). Scale bars, 25 μm. **e**, Distribution of YAP and TAZ localization presented as mean + s.e.m. for cells with more nuclear ($N > C$), more cytoplasmic ($N < C$), or even ($N = C$) distribution of YAP and TAZ. $n = 3$ biologically independent samples. Scale bars, 25 μm. **f**, RAP2 has an important role in adipocyte differentiation at low stiffness. Representative images of Oil-Red O staining of adipocyte-derived MSCs that were treated with adipocyte differentiation medium for 15 days. The MSCs were grown on 1 kPa hydrogels. Scale bars, 200 μm. **g**, Quantification of Oil-Red O-positive cells. The results are presented as mean ± s.e.m. Two-tailed *t*-test, $n = 8$ biological independent samples, $^{***}P = 0.00026$. **h**, CRISPR-mediated deletion of RAP2A, RAP2B and RAP2C in MCF7 and MDA-MB-468 by lentiviral transduction. The experiments were performed similarly to those in **c**. The images are representative of two independent experiments with similar results. **i**, RAP2 deletion promotes nuclear localization of YAP and TAZ in MCF7 cells at low stiffness. The images are from three independent experiments showing similar results. Merged, combined signals of YAP and TAZ (red), F-actin (green), and DAPI (blue). Scale bars, 25 μm. **j**, Quantification of YAP and TAZ localization in MCF7 cells. The distribution of YAP and TAZ localization is presented as mean + s.e.m. $n = 3$ biologically independent samples. **k**, YAP and TAZ are not significantly regulated by matrix stiffness in MDA-MB-468 cells. The images are from three independent experiments showing similar results. Merged, combined signals of YAP and TAZ (red), F-actin (green), and DAPI (blue). Scale bar, 25 μm. **l**, Quantification of YAP and TAZ localization in MDA-MB-468 cells. The distribution of YAP and TAZ localization is presented as mean + s.e.m. $n = 3$ biologically independent samples.

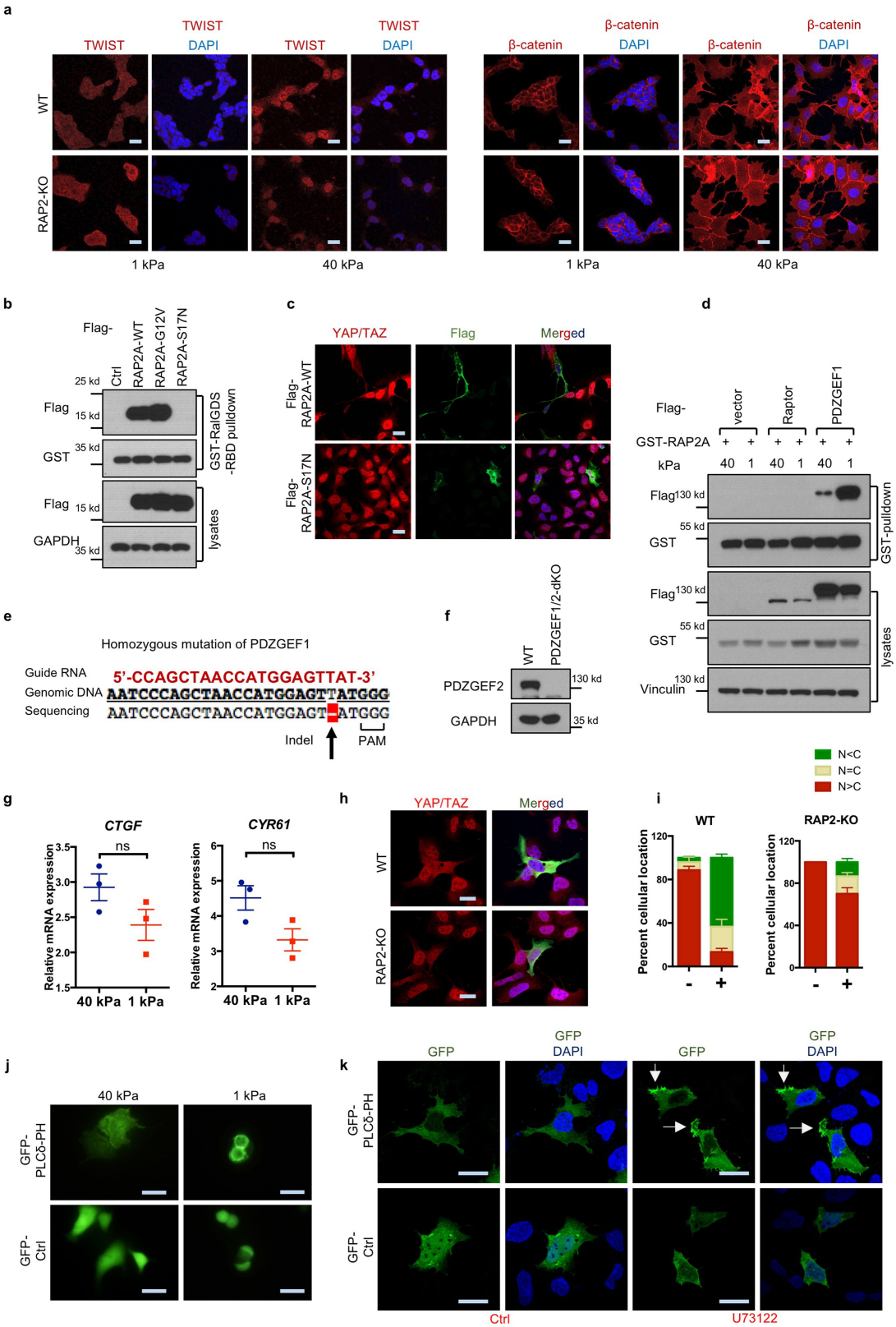

Extended Data Fig. 2 | See next page for caption.

Extended Data Fig. 2 | Activation of RAP2 at low matrix stiffness involves PDZGEF1 and PDZGEF2. a, RAP2 has no effect on localization of TWIST1 and β-catenin at different matrix rigidities. Immunofluorescence staining of TWIST1 and β-catenin in wild-type and RAP2-KO HEK293A cells grown on soft (1 kPa) and stiff (40 kPa) fibronectin-coated hydrogels. Low stiffness induced cytoplasmic localization of TWIST1 similarly in wild-type and RAP2-KO cells. Stiffness had no significant effect on β-catenin localization in HEK293A cells. Scale bars, 25 μm. The images are representative of three independent experiments with similar results. **b**, GST–RalGDS-RBD specifically binds to the active RAP2A in the pull-down assay. HEK293A cells were transfected with plasmids expressing wild-type RAP2A, RAP2A-G12V (constitutively GTP-binding), or RAP2A-S17N (GTP-binding deficient) and then seeded onto soft hydrogels. The cells were lysed 24 h after seeding and the lysates were incubated with glutathione agarose beads that were pre-loaded with GST–RalGDS-RBD. The beads were washed and subjected to western blot analyses with the indicated antibodies. The images are representative of two independent experiments with similar results. **c**, GTP-binding and activity of RAP2A is required to induce cytoplasmic translocation of YAP and TAZ. Merged, combined signals from YAP and TAZ (red), Flag (green), and DAPI (blue). Scale bar, 25 μm. The images are representative of two independent experiments with similar results. **d**, ECM stiffness regulates the interaction between RAP2A and PDZGEF1. GST–RAP2A plasmids were co-transfected with Flag–Raptor (a negative control) or Flag–PDZGEF1 into HEK293A cells. The cells were thereafter seeded on stiff and soft hydrogels. Twenty-four hours after seeding, the cells were lysed and the lysates were incubated with glutathione agarose beads for 6 h. Then the beads were washed and subjected to western blot analyses. The images are representative of two independent experiments with similar results. **e**, Sanger DNA sequencing confirmed the homozygous deletion of a 'T' nucleotide in PDZGEF1 genomic DNAs in PDZGEF1/2-dKO HEK293A cells. **f**, Western blot showing the absence of PDZGEF2 expression in PDZGEF1/2-dKO HEK293A cells. The images are representative of two independent experiments with similar results. **g**, The repression of the YAP and TAZ target genes *CTGF* and *CYR61* by low stiffness was compromised in PDZGEF1/2-dKO cells. Expression of *CTGF* and *CYR61* in PDZGEF1/2-dKO HEK293A cells on soft and stiff matrices was measured by qPCR. ns, not significant, two-tailed *t*-test, $n = 3$ biologically independent samples. Data are represented as mean ± s.e.m. **h**, RAP2 is required for PDZGEF1 to induce cytoplasmic localization of YAP and TAZ. Immunofluorescence showing localization of YAP and TAZ after ectopic expression of Flag-tagged PDZGEF1 in wild-type and RAP2-KO cells at high stiffness. Merged, combined signals from Flag-PDZGEF1 (green), YAP and TAZ (red), and DAPI (blue). Scale bars, 25 μm. **i**, Quantification of the results in **h**. + denotes Flag–PDZGEF1-transfected cells, – denotes cells that were not transfected. Data are represented as mean + s.e.m. $n = 3$ biologically independent samples. **j**, Stiffness influences cellular PtdIns(4,5)P_2. The PtdIns(4,5)P_2 reporter GFP–PLCδ-PH domain, which binds to PtdIns(4,5)P_2, was imaged with a Nikon inverted microscope in cells at low or high stiffness. Cells grown at high stiffness display diffuse PtdIns(4,5)P_2 localization whereas cells at low stiffness show enrichment of PtdIns(4,5)P_2 at the plasma membrane. The image is representative of two independent experiments with similar results. Scale bars, 25 μm. **k**, Inhibition of PLC alters cellular PtdIns(4,5)P_2 distribution. Immunofluorescence of cells treated with 5 μM PLC inhibitor U73122 at high stiffness. GFP was detected with anti-GFP immunofluorescence. PtdIns(4,5)P_2 enrichment, indicated by arrows, was observed. Scale bars, 25 μm. The image is representative of two independent experiments with similar results.

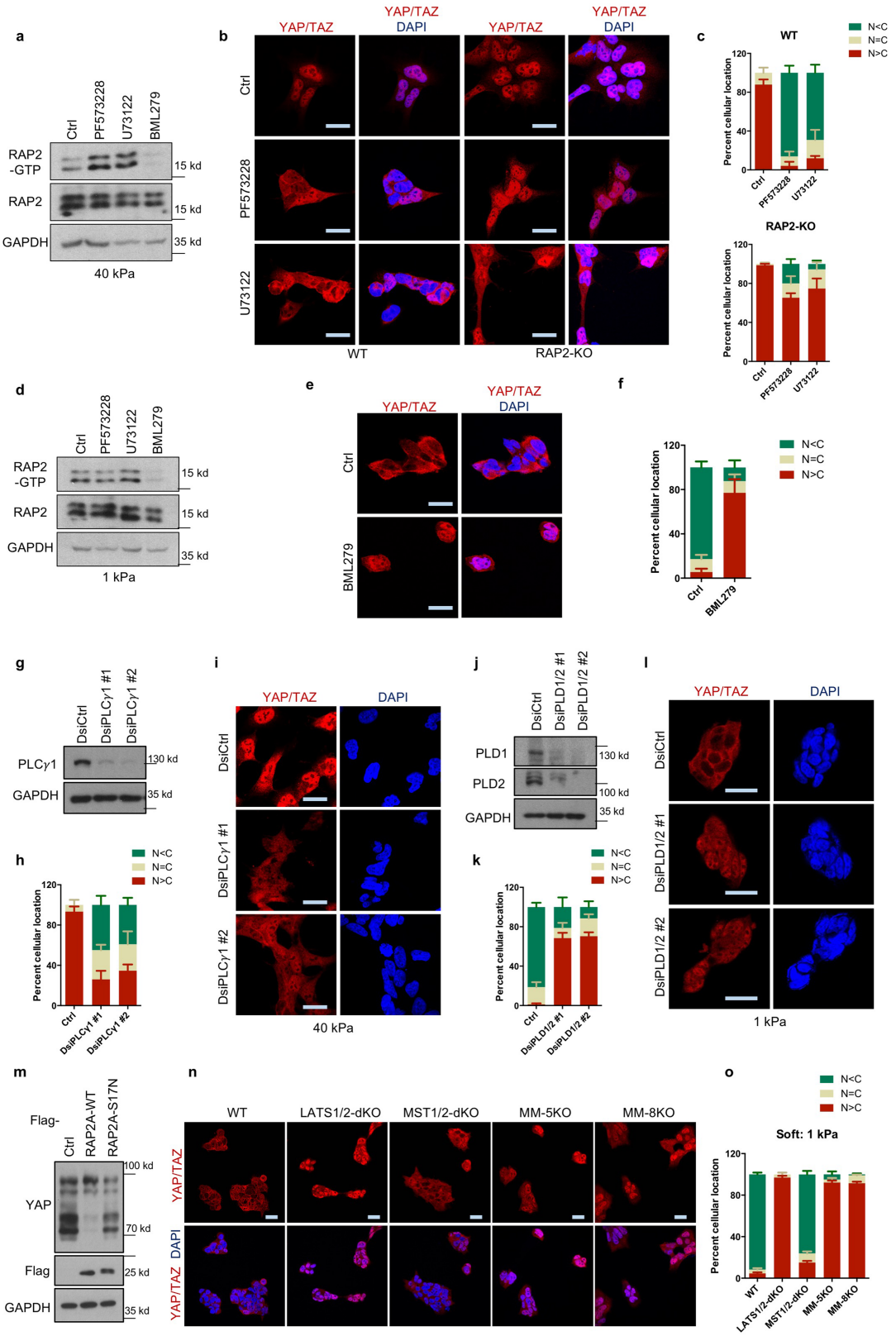

Extended Data Fig. 3 | See next page for caption.

Extended Data Fig. 3 | FAK, PLCγ1, and PLD are involved in RAP2 activation and Hippo pathway activation in response to stiffness. a, The FAK inhibitor PF573228 and PLC inhibitor U73122 promote RAP2–GTP loading at high stiffness. The images are representative of two biologically independent experiments with similar results. **b**, RAP2 functions downstream of FAK and PLC to regulate localization of YAP and TAZ. YAP and TAZ were imaged in cells cultured at high stiffness and treated with 10 μM FAK inhibitor PF573228 or 5 μM PLC inhibitor U73122. Scale bars, 25 μm. The image is representative of three (wild-type treated with PF573228 or U73122; RAP2-KO control (Ctrl)) or four (wild-type control; RAP2-KO treated with PF573228 or U73122) biologically independent samples with similar results. **c**, Distribution of localization from **b** as mean + s.e.m. $n = 3$ (wild-type treated with PF573228 or U73122; RAP2-KO control) or four (wild-type control; RAP2-KO treated with PF573228 or U73122) biologically independent samples. **d**, The PLD1 and PLD2 inhibitor BML279 suppresses RAP2–GTP binding at low stiffness. The images are representative of two independent experiments with similar results. **e**, Inhibition of PLD increases nuclear YAP and TAZ in cells at low stiffness. Cells growing at low stiffness were treated with 5 μM PLD inhibitor BML279. Scale bars, 25 μm. Images are representative of seven (control) or five (BM279) biologically independent samples with similar results. **f**, Distribution of localization from **e** presented as mean + s.e.m. $n = 7$ (control) or 5 (BML279) biologically independent samples. **g**, Western blot showing PLCγ1 knockdown by duplex siRNAs (DsiRNAs). Two independent siRNAs were used. The image is representative of two independent experiments with similar results. **h**, PLCγ1 knockdown decreases nuclear YAP and TAZ at high stiffness. Quantification of YAP and TAZ localization in PLCγ1 knockdown and control cells growing on 40 kPa hydrogels. The distribution of YAP and TAZ localization is presented as mean + s.e.m. $n = 3$ biologically independent samples. **i**, Representative images of YAP and TAZ localization in cells with PLCγ1 knockdown. Scale bars, 25 μm. The images are representative of three biologically independent experiments with similar results. **j**, Western blot showing knockdown of PLD1 and PLD2. Two independent DsiRNAs were used. The image is representative of two independent experiments with similar results. **k**, Knockdown of PLD1 and PLD2 increases nuclear YAP and TAZ at low stiffness. Quantification of YAP and TAZ localization in PLD1/2 knockdown and control cells growing on 1 kPa hydrogels. The distribution of YAP and TAZ localization is presented as mean + s.e.m. The results are from three biologically independent samples. **l**, Representative images of YAP and TAZ localization in PLD1/2 knockdown cells. Scale bars, 25 μm. Images are representative of three biologically independent experiments with similar results. **m**, Wild-type, but not GTP-binding-deficient (S17N), RAP2A induces YAP phosphorylation. YAP phosphorylation was analysed by phos-tag SDS–PAGE in HEK293A cells stably expressing wild-type or S17N mutant RAP2A at high stiffness. Images are representative of two independent experiments with similar results. **n**, Hippo pathway components are involved in regulation of YAP and TAZ by stiffness. HEK293A cell lines in which Hippo components were deleted were cultured at low stiffness (1 kPa). Deletion of Hippo components includes LATS1/2-dKO, MST1/2-dKO, MM-5KO (MST1/2-MAP4K4/6/7-5KO), and MM-8KO (MST1/2-MAP4K1/2/3/4/6/7-8KO). Images are representative of three biologically independent experiments with similar results. Scale bars, 25 μm. **o**, Quantification of immunofluorescence of the samples in **n**. The distribution of YAP and TAZ localization is presented as mean + s.e.m. $n = 3$ biologically independent samples.

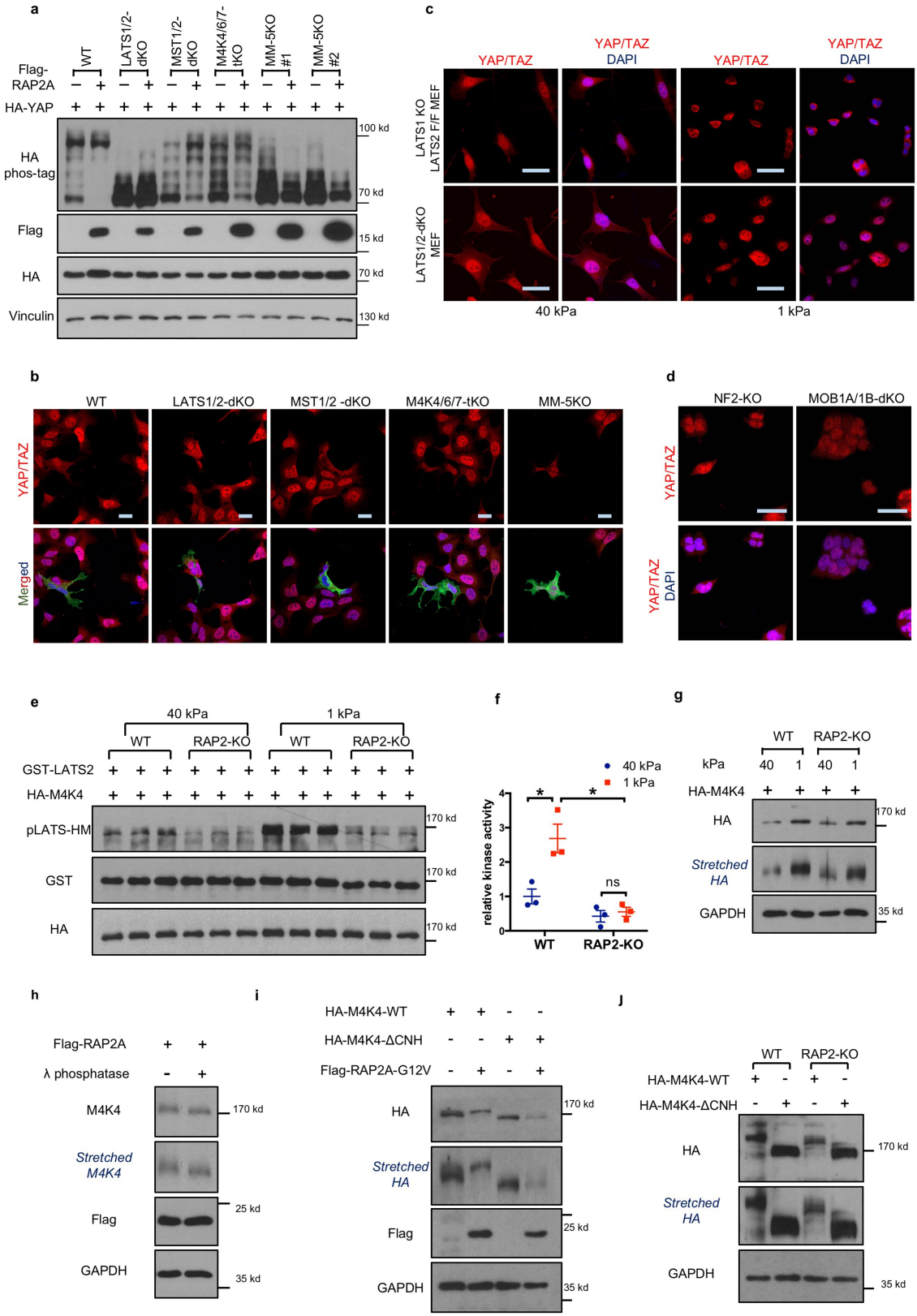

Extended Data Fig. 4 | See next page for caption.

Extended Data Fig. 4 | RAP2 activates MAP4K4 and induces phosphorylation of YAP. a, Hippo pathway components are required for RAP2A to induce phosphorylation of YAP and TAZ. RAP2A is overexpressed in the indicated knockout HEK293A cells. Images are representative of two independent experiments with similar results. Two clones of MM-5KO cells were used for this experiment. **b**, RAP2A acts through the Hippo pathway to induce cytoplasmic localization of YAP and TAZ. Flag–RAP2A was transfected into HEK293A cell lines with deletion of different core Hippo pathway components as indicated. Localization of YAP and TAZ was analysed by immunofluorescence. Merged, combined signals from Flag–RAP2A (green), YAP and TAZ (red), and DAPI (blue). Scale bars, 25 μm. Images are representative of three biologically independent experiments with similar results. **c**, Localization of YAP and TAZ in *LATS1*$^{-/-}$*LATS2*$^{flox/flox}$ (LATS1-KO LATS2-F/F) and *LATS1*$^{-/-}$*LATS2*$^{-/-}$ (LATS1/2-dKO) mouse embryonic fibroblasts (MEFs). Scale bars, 25 μm. Images are representative of two biologically independent experiments with similar results. **d**, Localization of YAP and TAZ in NF2-KO and MOB1A/1B-dKO HEK293A cells. Scale bars, 25 μm. Images are representative of two biologically independent experiments with similar results. **e**, Low matrix stiffness activates MAP4K4 in a RAP2-dependent manner. Plasmids expressing HA-tagged MAP4K4 were transfected into wild-type and RAP2-KO HEK293A cells. Twenty-four hours after seeding on 40 kPa or 1 kPa hydrogels, HA–MAP4K4 proteins were immunoprecipitated and then used for an in vitro kinase assay, in which recombinant full-length GST-tagged LATS2 protein was used as a substrate. Phosphorylation of LATS2 by MAP4K4 was detected with a phosphospecific antibody recognizing the phosphorylated hydrophobic motif of LATS1 and LATS2. Results are from three biologically independent experiments. **f**, Quantification of the kinase assay (**e**) shown as mean ± s.e.m. Relative LATS2 phosphorylation was normalized to protein levels of HA–MAP4K4 and defined as MAP4K4 kinase activity. $n = 3$ biologically independent samples, two-tailed t-test, $^{*}P = 0.027$ (wild-type, 1 kPa versus RAP2 KO, 1 kPa) or 0.037 (wild-type, 1 kPa versus wild-type, 40 kPa); ns, not significant. **g**, The lysates of wild-type and RAP2-KO HEK293A cells growing on stiff and soft hydrogels were analysed by western blot for MAP4K4 migration. A 'stretched' image was generated by vertically extending the same western image directly above it in order to better visualize the MAP4K4 mobility shift. The image is representative of two independent experiments with similar results. **h**, Phosphatase treatment increases MAP4K4 migration on SDS–PAGE. Lambda phosphatase was used to treat cell lysates of RAP2A-expressing HEK293A cells before western blotting. These results indicate that the altered migration of MAP4K4 was correlated with its phosphorylation. The image is representative of two independent experiments with similar results. **i**, RAP2A promotes MAP4K4 phosphorylation (slower band migration) dependent on its citron domain. Flag–RAP2A-G12V plasmid was co-transfected with wild-type MAP4K4 or the citron domain deletion mutant (ΔCNH) into HEK293A cells. The image is representative of two independent experiments with similar results. **j**, RAP2 is required for the reduction in MAP4K4 mobility. Wild-type and ΔCNH mutant MAP4K4 were transfected into wild-type and RAP2-KO HEK293A cells. The image is representative of two independent experiments with similar results.

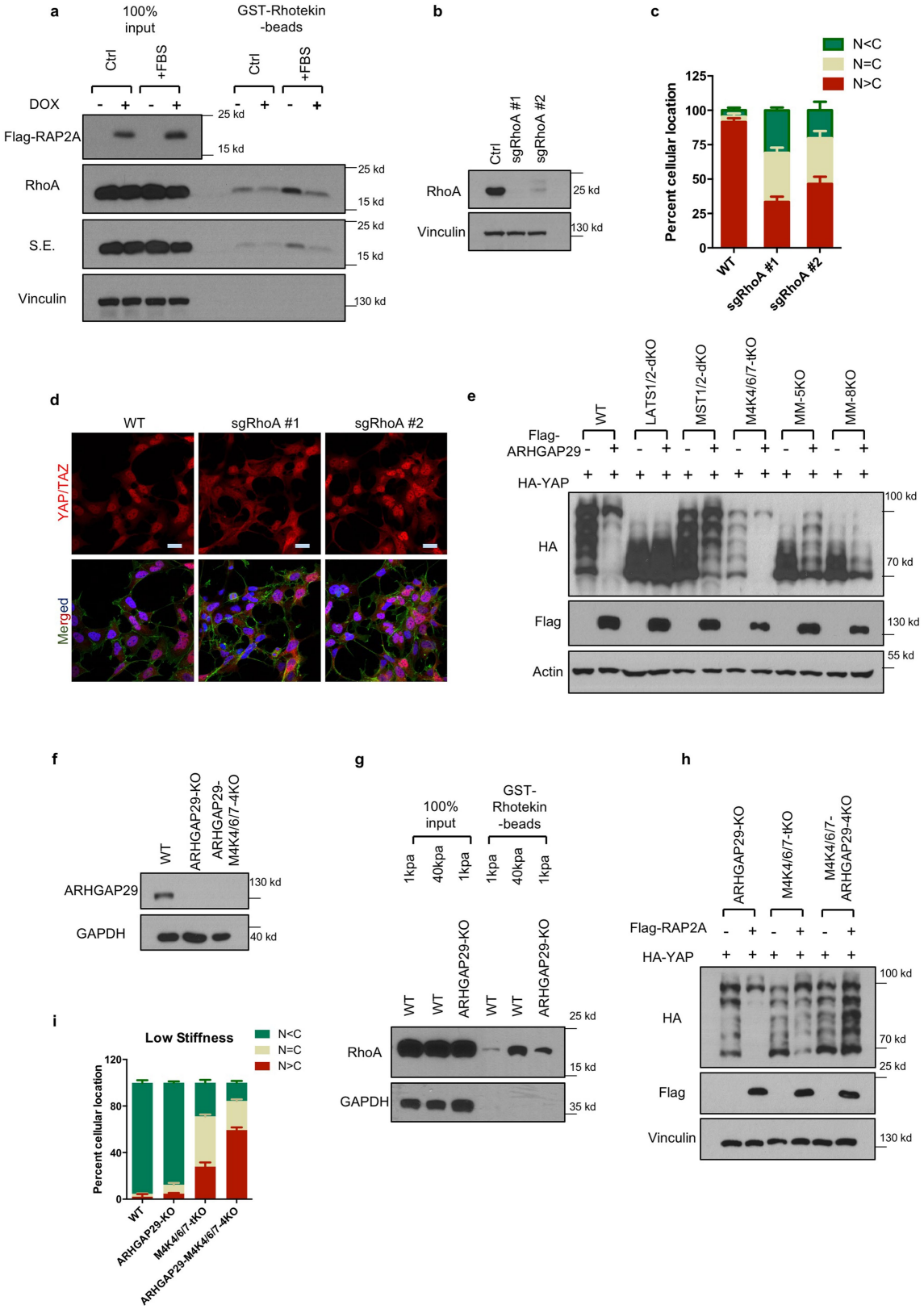

Extended Data Fig. 5 | See next page for caption.

Extended Data Fig. 5 | RAP2 inhibits RhoA GTPase through ARHGAP29. a, RAP2A expression inhibits endogenous RhoA GTP-binding. HEK293A cells with doxycycline-inducible expression of RAP2A were established and the expression of Flag–RAP2A was induced by doxycycline. RhoA activity was determined by a GST–Rhotekin-RBD pull-down assay. s.e. denotes short exposure of the RhoA western blot. The image is representative of two independent experiments with similar results. **b**, Western blot confirms CRISPR-mediated RhoA gene editing. HEK293A cells were transfected with CRISPR plasmids targeting RhoA and selected with puromycin for 3 days. Two sgRNAs were used to generate two RhoA knockout pools (sgRhoA #1 and #2)[16]. The image is representative of two independent experiments with similar results. **c**, CRISPR-mediated deletion of RhoA leads to increased cytoplasmic localization of YAP and TAZ in HEK293A cells at high stiffness. The localization distribution is presented as mean + s.e.m. $n = 6$ biologically independent samples. **d**, Representative immunofluorescence images from **c**. Scale bars, 25 μm. **e**, ARHGAP29 induces YAP phosphorylation in a Hippo pathway-dependent manner. MM-5KO, a HEK293A clone with deletion of MST1, MST2, MAP4K4, MAP4K6 and MAP4K7. MM-8KO, deletion of MST1, MST2, MAP4K1, MAP4K2, MAP4K3, MAP4K4, MAP4K6 and MAP4K7. YAP phosphorylation was detected by phos-tag gels. The image is representative of two independent experiments with similar results. **f**, Immunoblot showing deletion of ARHGAP29 in HEK293A wild-type and MAP4K4/6/7-tKO cells. The image is representative of two independent experiments with similar results. **g**, Deletion of ARHGAP29 compromises inhibition of RhoA by low matrix stiffness. Wild-type and ARHGAP29-KO HEK293A cells were cultured at the indicated stiffness and then assayed for RhoA activity with a GST–Rhotekin-RBD binding assay. The image is representative of two independent experiments with similar results. **h**, Combined deletion of ARHGAP29, MAP4K4, MAP4K6 and MAP4K7 abolishes YAP phosphorylation induced by RAP2A. HA–YAP was co-transfected with vector or Flag–RAP2A into HEK293A cells cultured at high stiffness. HA–YAP phosphorylation was detected by phos-tag SDS–PAGE. The image is representative of two independent experiments with similar results. **i**, Combined deletion of ARHGAP29, MAP4K4, MAP4K6 and MAP4K7 blocks low stiffness-induced cytoplasmic localization of YAP. Quantification of YAP and TAZ localization in HEK293A cells with deletion of ARHGAP29 and/or MAP4K4, MAP4K6 and MAP4K7 at low stiffness in Fig. 3e. The YAP and TAZ localization distribution is presented as mean + s.e.m. $n = 3$ biologically independent samples.

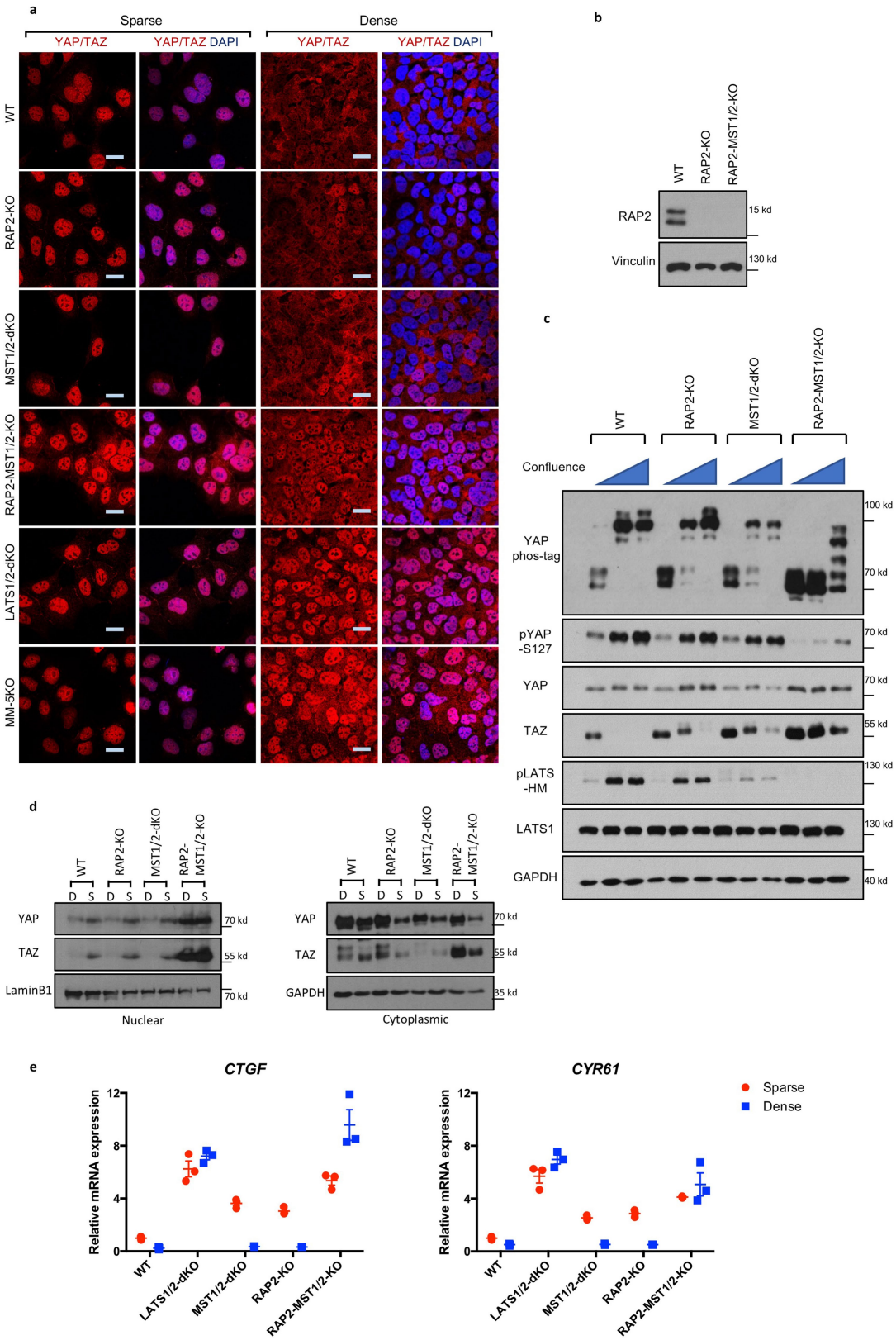

Extended Data Fig. 6 | See next page for caption.

Extended Data Fig. 6 | RAP2 contributes to cell density-induced inactivation of YAP and TAZ. a, Cytoplasmic translocation of YAP and TAZ caused by cell contact involves RAP2 and the Hippo pathway. Scale bars, 25 μm. MM-5KO, a HEK293A clone with deletion of MST1, MST2, MAP4K4, MAP4K6 and MAP4K7. RAP2-MST-KO, deletion of RAP2A, RAP2B, RAP2C, MST1 and MST2. The images are representative of three biologically independent experiments with similar results. **b**, Western blot showing absence of RAP2 proteins in RAP2-KO and RAP2-MST1/2-KO cells. Note that part of these results is shown in Fig. 1b and are from the same experiment. The image is representative of two independent experiments with similar results. **c**, Phosphorylation of YAP and TAZ induced by cell contact requires RAP2, MST1 and MST2. The western blot shows phosphorylation of YAP in cells with low, medium, or high confluence. The image is representative of two independent experiments with similar results. **d**, Deletions of RAP2A, RAP2B, RAP2C, MST1 and MST2 interfere with regulation of YAP and TAZ by cell density. Subcellular fractionations were performed for wild-type, RAP2-KO, MST1/2-dKO and RAP2-MST1/2-KO HEK293A cells cultured at low (S, sparse) or high density (D, dense). GAPDH and LaminB1 are markers for the cytoplasmic and nuclear fraction, respectively. The image is representative of two independent experiments with similar results. **e**, RAP2A, RAP2B, RAP2C, MST1 and MST2 are required for regulation of YAP and TAZ target genes by cell density. qPCR was performed to determine the expression of the YAP and TAZ target genes *CTGF* and *CYR61* in the above cells at low or high confluence. Data are represented as mean ± s.e.m. $n = 3$ biologically independent samples.

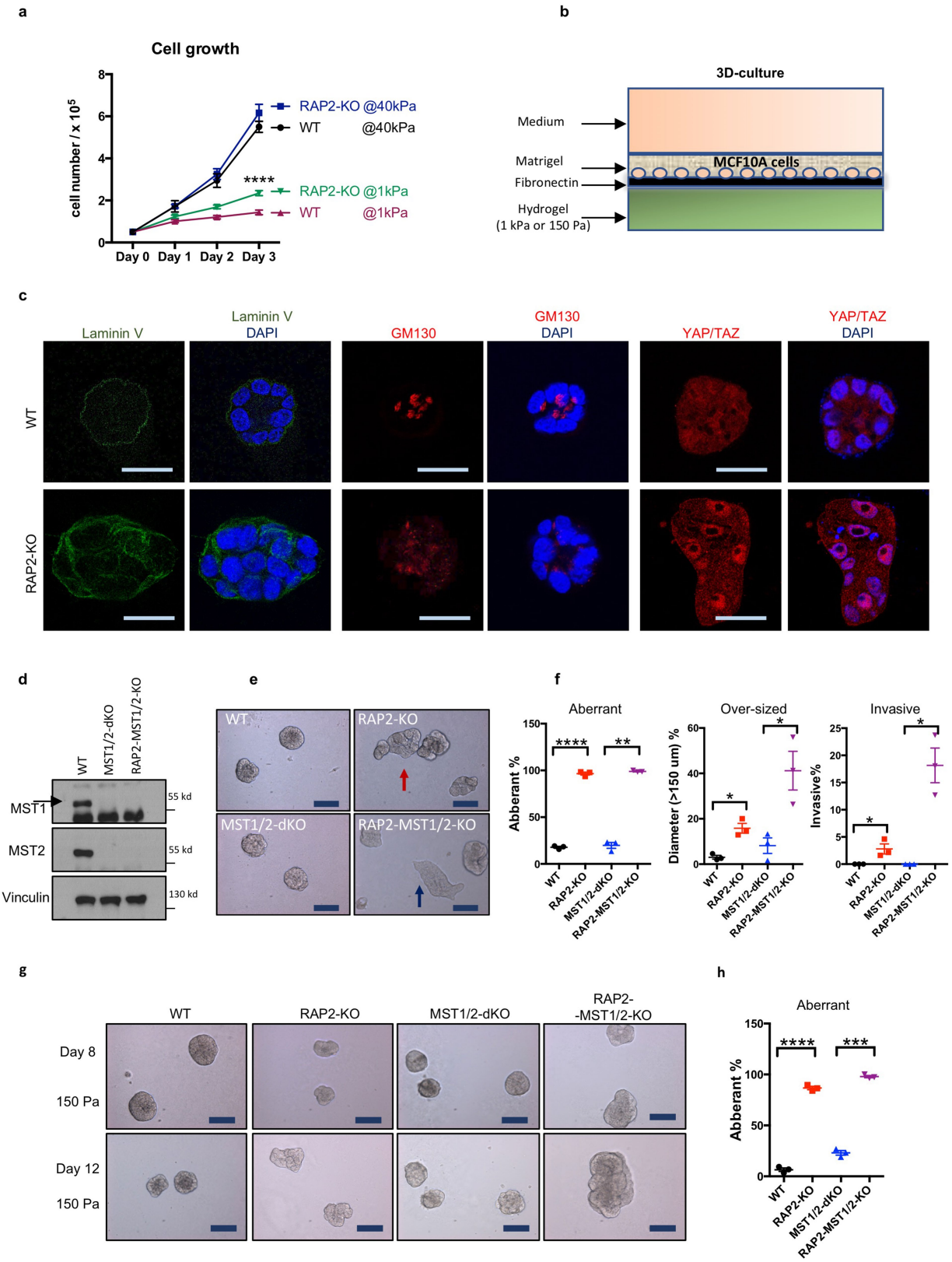

Extended Data Fig. 7 | See next page for caption.

Extended Data Fig. 7 | RAP2 prevents aberrant acinus growth in MCF10A cells on soft matrices. a, RAP2 deletion selectively enhances HEK293A cell growth on soft matrices. Wild-type and RAP2-KO HEK293A cells were seeded on stiff or soft matrices, and cell numbers were recorded as mean ± s.e.m. every day. Two-way ANOVA test, $^{****}P < 0.0001$, wild-type versus RAP2-KO cells cultured at 1 kPa, $n = 3$ biologically independent samples. **b**, Model of 3D culture of MCF10A cells. **c**, RAP2 deletion causes abnormal acinus growth and cell polarity defects in MCF10A cells. Immunofluorescence staining of acini for cell polarity markers, Laminin V and GM130, and YAP and TAZ in wild-type and RAP2-KO MCF10A cells cultured for 6 days. Scale bars, 25 μm. Images are representative of three independent experiments with similar results. **d**, Western blot showing deletion of MST1 and MST2 in wild-type and RAP2-KO cells. The arrow indicates the specific band for MST1. The image is representative of two independent experiments with similar results. **e**, Representative images showing acinus formation by various genetically engineered MCF10A cells at 1 kPa. The red arrow indicates aberrant acini. The blue arrow indicates invasive cell morphology. Scale bars, 100 μm. The results are representative of two independent experiments with similar results. **f**, Quantification of aberrant, oversized, and invasive acini in **e**. The percentage of the cells is presented as mean ± s.e.m. Two-tailed *t*-tests were used for statistical analyses of aberrant and oversized clones in $n = 3$ biologically independent samples. Aberrant: $^{****}P = 0.0000062$; $^{***}P = 0.0012$; oversized: $^{*}P = 0.017$ (wild-type versus RAP2-KO) or 0.046 (MST1/2-dKO versus RAP2-MST1/2-KO). For analysis of invasive clones, one-tailed *t*-test was used as no invasive clones were observed in either wild-type or MST1/2-dKO cells. $^{*}P = 0.047$ (wild-type versus RAP2-KO) or 0.029 (MST1/2-dKO versus RAP2-MST1/2-KO). $n = 3$ biologically independent samples. **g**, Representative images showing acinus formation by various genetically engineered MCF10A cells at 150 Pa. Scale bars, 100 μm. Images are representative of two biologically independent experiments with similar results. **h**, Quantification of aberrant acini in **g**. The results are from three biologically independent samples. Two-tailed *t*-tests were used for statistical analyses of aberrant clones in $n = 3$ biologically independent samples. $^{****}P = 0.000045$; $^{***}P = 0.00011$.

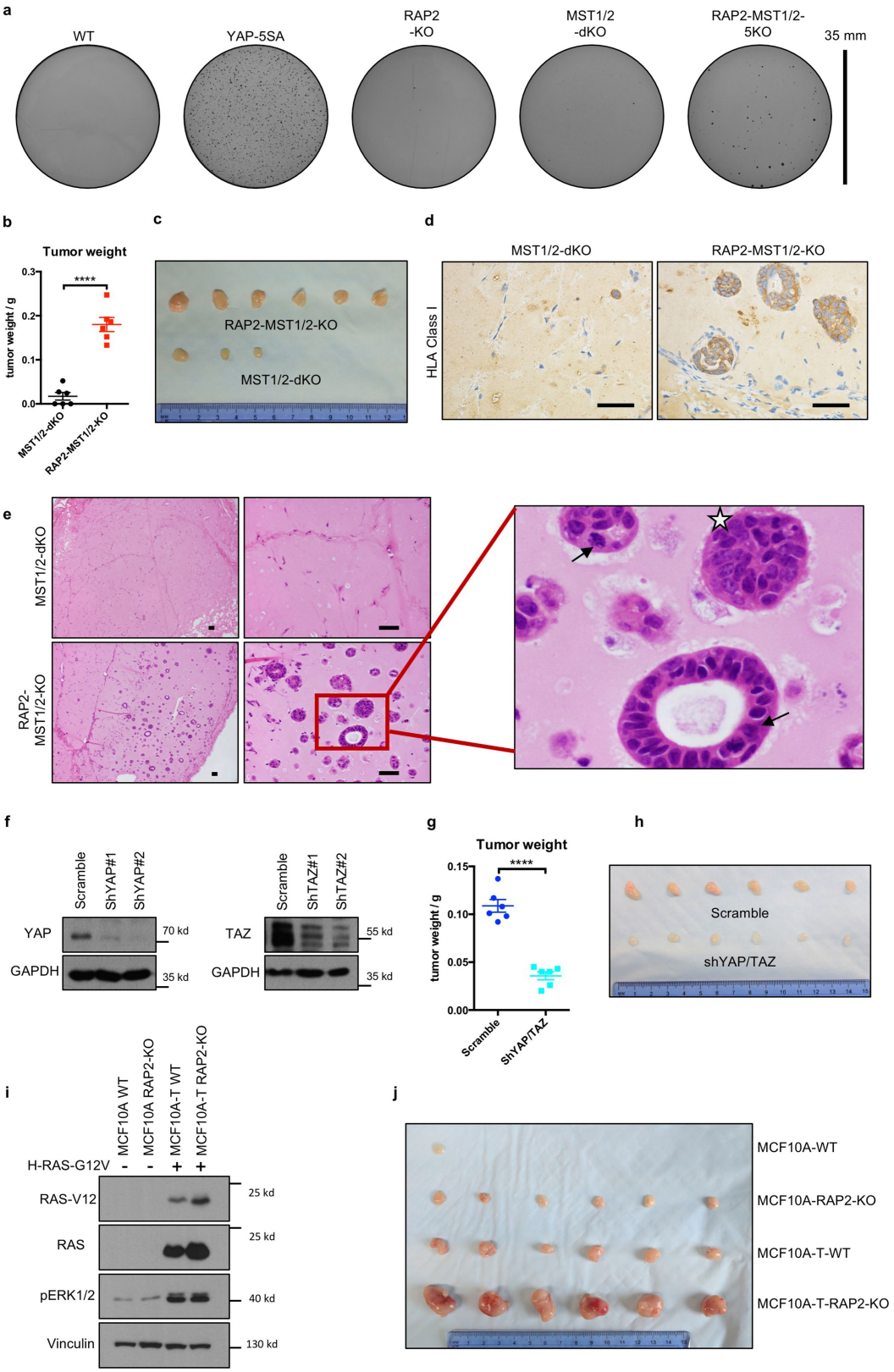

Extended Data Fig. 8 | See next page for caption.

Extended Data Fig. 8 | RAP2 deletion contributes to aberrant acinus growth and tumorigenesis of MCF10A cells in a YAP- and TAZ-dependent manner. a, Representative images showing soft-agar assays of MCF10A cells. Overexpression of the constitutively active YAP(5SA) (mutation of all five LATS1- and LATS2-phosphorylation serines to alanines in YAP) strongly promotes anchorage-independent growth. Combined deletion of RAP2, MST1 and MST2, but not either group alone, also causes anchorage-independent growth of MCF10A cells. Images are representative of three biologically independent experiments with similar results. Scale bar, 35 mm. **b**, RAP2 inhibits tumorigenicity of MST1/2-dKO MCF10A cells. MST1/2-dKO and RAP2-MST1/2-KO MCF10A cells were injected into NOD/SCID mice. Tumour weight on day 32 after injection is presented as mean ± s.e.m. $n = 6$ biologically independent xenografts, $^{****}P = 0.000025$, two-tailed t-test. **c**, Representative tumour sizes. Only three very small xenografts were recovered from the initial 6 subcutaneous injections for MST1/2-dKO cells. Images representative of six biologically independent xenografts for each group that were initially made in the NOD/SCID mice. **d**, Immunohistochemistry staining with an antibody recognizing human HLA Class I. Only the acinus structures in the xenografts were formed by MCF10A cells. Stroma cells negative for HLA class I were derived from the host mice. Images are representative of two biologically independent experiments with similar results. Scale bars, 50 μm. **e**, Haematoxylin and eosin staining of xenografts from MST1/2-dKO MCF10A cells shows that largely hypocellular connective tissue is observed as stroma from the host animals. By contrast, RAP2-MST1/2-KO xenografts showed MCF10A cell-derived acinar and duct structures exhibiting nuclear polymorphisms, irregular nuclear contour, hyperchromasia, prominent nucleoli (star), and pathological mitosis (arrows). Images representative of two biologically independent experiments with similar results. Scale bars, 50 μm. **f**, Western blot showing knockdown of YAP or TAZ by lentiviral shRNAs in RAP2-MST1/2-KO MCF10A cells. shYAP#2 and shTAZ#1 were used for the xenograft studies. The image is representative of two independent experiments with similar results. **g**, Knockdown of YAP and TAZ inhibits tumour growth of RAP2-MST1/2-KO MCF10A cells. Tumour weight on day 32 is presented as mean ± s.e.m. Two-tailed t-test, $n = 6$, $^{****}P = 0.000010$. **h**, Xenografts from NOD/SCID mice, in which six biologically independent xenografts were generated for each group. **i**, Western blot showing that MCF10A-T cells are generated by expression of the oncogenic mutant H-RAS-G12V. H-RAS-G12V expression activates ERK whereas RAP2 deletion has no effect on ERK. The comparable phosphorylation levels of ERK1 and ERK2 in wild-type and RAP2-KO MCF10A-T cells indicate that the difference in xenograft growth was not due to difference in ERK1 and ERK2 activity. Image representative of two independent experiments with similar results. **j**, MCF10A and MCF10A-T xenografts from nude mice, in which six biologically independent xenografts were generated for each group and yielded similar results.

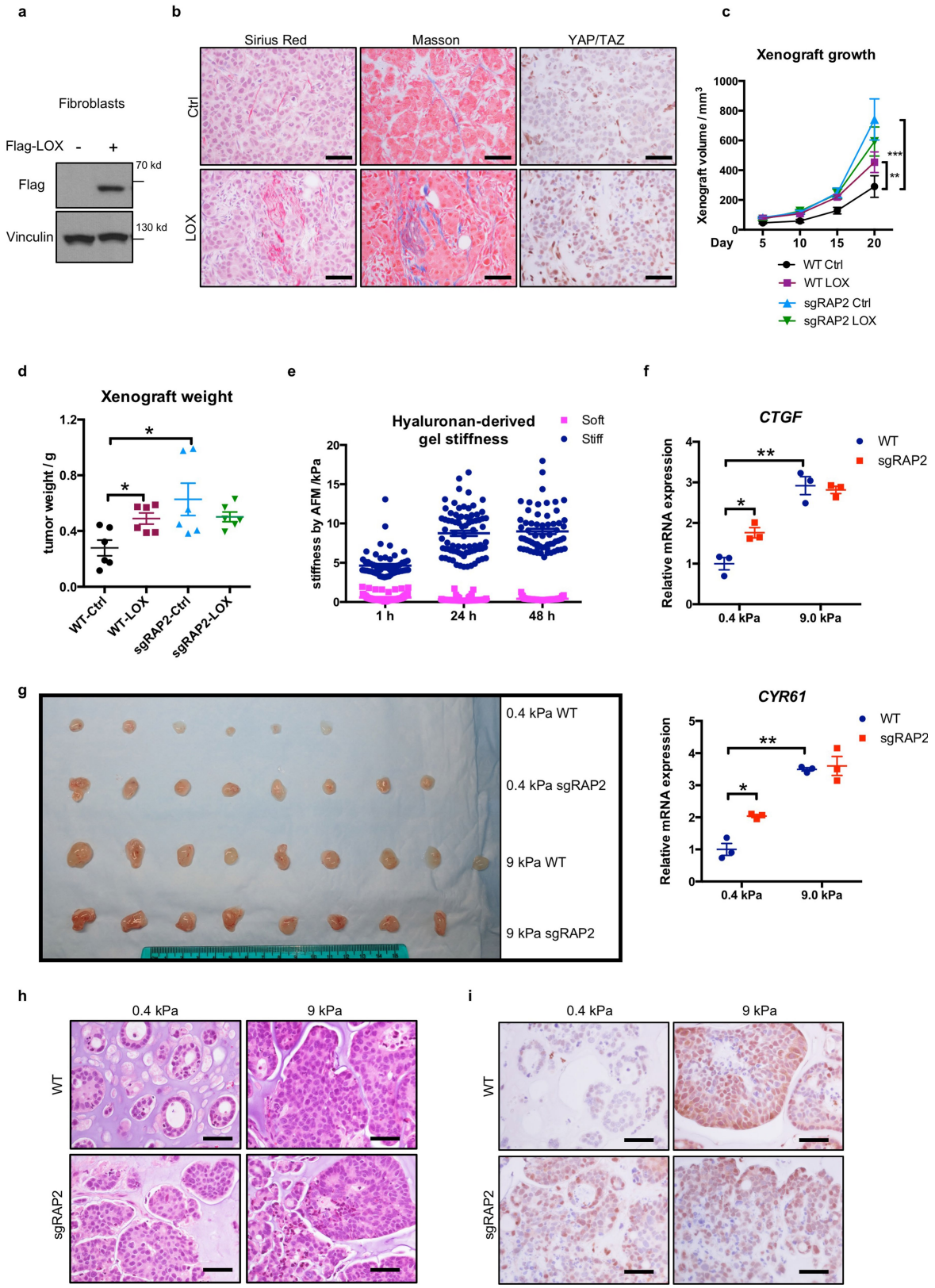

Extended Data Fig. 9 | See next page for caption.

Extended Data Fig. 9 | RAP2 deletion selectively promotes MCF7 malignancy at low stiffness in vivo. a, Western blot showing LOX overexpression in NIH3T3 fibroblasts. Ectopic LOX expression promotes cross-linking of ECM proteins and thus increases matrix stiffness[28]. Image representative of two independent experiments with similar results. **b**, RAP2 is involved in the xenograft growth enhancement caused by LOX-overexpressing fibroblasts. Xenografts were generated by co-injection of 0.4×10^6 fibroblasts (control and Flag–LOX-overexpressing) and 2.0×10^6 MCF7 cells. The xenografts were removed on day 6 and examined for collagen deposition and crosslinking and localization of YAP and TAZ. LOX overexpression led to a woven-like structure of collagen in the xenografts based on Sirius Red staining (red colour for collagen) and Masson staining (blue colour for collagen), and increased nuclear YAP and TAZ. Images representative of three biologically independent experiments with similar results. Scale bars, 50 μm. **c**, LOX-induced tumour growth requires RAP2. Xenografts were generated by co-injection of 0.4×10^6 NIH3T3 cells and 2.0×10^6 MCF7 cells. The growth of the xenografts with different combinations of NIH3T3 and MCF7 cells is shown as mean ± s.e.m. Deletion of RAP2A, RAP2B and RAP2C promoted MCF7 tumour growth and masked the enhancement induced by co-injected LOX-expressing fibroblasts. **two-way ANOVA test (wild-type MCF7 + wild-type NIH3T3 cells versus wild-type MCF7 +LOX-overexpressing NIH3T3 cells), $n = 6$ biologically independent samples, $P = 0.0027$. ***two-way ANOVA test (sgRAP2 MCF7 + wild-type NIH3T3 cells versus wild-type MCF7 + wild-type NIH3T3 cells), $n = 6$ biologically independent samples, $P = 0.002$. **d**, Tumour weights (mean ± s.e.m.). *two-tailed *t*-test, $n = 6$ biologically independent xenografts, $P = 0.014$ (wild-type MCF7 + wild-type NIH3T3 cells versus wild-type MCF7 + LOX-overexpressing NIH3T3 cells) or 0.029 (sgRAP2 MCF7 + wild-type NIH3T3 cells versus wild-type MCF7 + wild-type NIH3T3 cells). **e**, The elasticity or stiffness of the 'soft' and 'stiff' semi-synthetic hyaluronan-derived gels was measured by atomic force microscopy. Results presented as mean ± s.e.m. The measurements were made more than 55 times for each stiffness at each time. **f**, RAP2 inhibits expression of the YAP and TAZ target genes *CTGF* and *CYR61* at low stiffness but not at high stiffness. Quantitative real-time PCR analyses of *CTGF* and *CYR61* in wild-type and sgRAP2 MCF7 cells (as in Extended Data Fig. 1g) cultured in vitro for 48 h in soft or stiff hyaluronan gel. Relative mRNA levels presented as mean ± s.e.m. $n = 3$ biologically independent samples, two-tailed *t*-test. For *CTGF*, *sgRAP2 versus wild-type at 0.4 kPa, $P = 0.020$; **0.4 kPa versus 9.0 kPa for wild-type, $P = 0.0032$. For *CYR61*, *sgRAP2 versus wild-type, $P = 0.025$; **0.4 kPa versus 9.0 kPa for wild-type, $P = 0.0033$. **g**, Xenograft tumours. For wild-type cells grown at 0.4 kPa, eight independent xenografts were initially generated in nude mice. However, owing to animal deaths, only six xenografts were recovered. For wild-type cells grown at 9 kPa, nine independent xenografts were generated. For sgRAP2 cells grown at both 0.4 kPa and 9 kPa, eight independent xenografts were generated. **h**, RAP2 deletion preferentially promotes MCF7 malignancy at low stiffness. MCF7 xenografts stained with haematoxylin and eosin. Wild-type cells embedded in 0.4 kPa matrix produced mostly tubular and some cribriform structures whereas those embedded in 9 kPa matrix produced mostly solid nests, as well as more marked cellular pleomorphism and nuclear atypia. sgRAP2 cells showed more malignant architecture and morphology at 0.4 ka, while at high stiffness (9 kPa) sgRAP2 and wild-type cells exhibited similar morphology. Images representative of three biologically independent experiments with similar results. Scale bars, 50 μm. **i**, Immunohistochemistry for YAP and TAZ in xenografts. RAP2 deletion increased nuclear YAP and TAZ. Images representative of three biologically independent experiments with similar results. Scale bars, 50 μm.

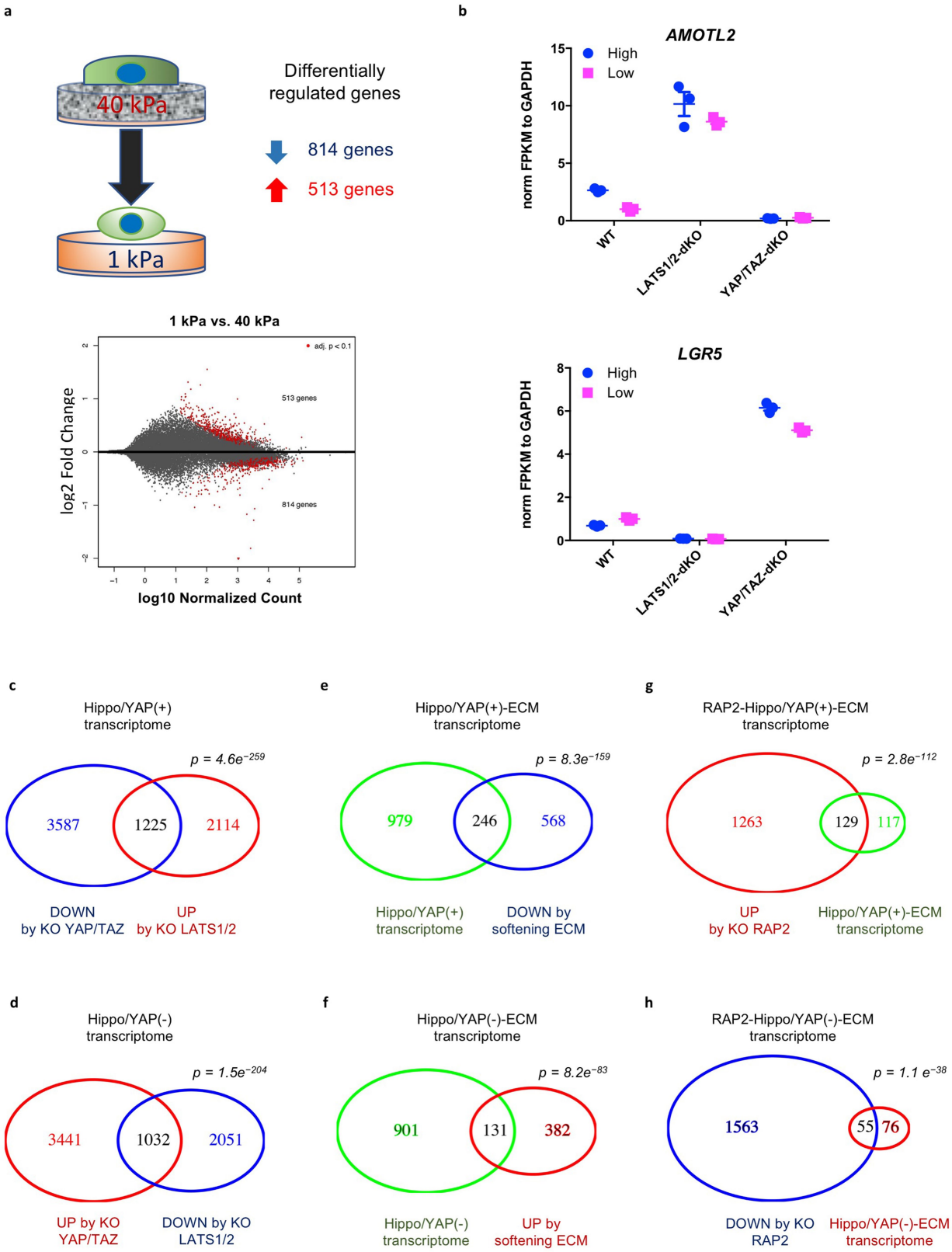

Extended Data Fig. 10 | See next page for caption.

Extended Data Fig. 10 | RAP2 mediates regulation of the ECM stiffness transcriptome by the Hippo pathway. a, MA plot of wild-type cells in low stiffness versus wild-type cells in high stiffness. Three biologically independent samples were assayed for each condition. Differentially expressed genes (adjusted *P* value <0.1) are coloured red. P values for deferential expression were derived using the Wald test and corrected using the Benjamini–Hochberg procedure with default functions in DESeq2. **b**, Dot plot showing expression of *AMOTL2* and *LGR5*. *AMOTL2* and *LGR5* are YAP- and TAZ-dependent and stiffness-regulated genes. High and low denote high stiffness (40 kPa) and low stiffness (1 kPa). Data are presented as mean $\pm$ s.e.m. $n = 3$ biologically independent samples. **c**, Venn diagram comparing genes downregulated by YAP and TAZ knockout at high stiffness and genes upregulated by LATS1 and LATS2 knockout at low stiffness. **d**, Venn diagram comparing genes upregulated by YAP and TAZ knockout at high stiffness and genes downregulated by LATS1 and LATS2 knockout at low stiffness. **e**, Venn diagram comparing overlapping genes from **c** and genes downregulated by low stiffness. **f**, Venn diagram comparing overlapping genes from **d** and genes upregulated by low stiffness. **g**, Venn diagram comparing overlapping genes from **e** and genes upregulated by RAP2 knockout at low stiffness. **h**, Venn diagram comparing overlapping genes from **f** and genes downregulated by RAP2 knockout at low stiffness. *P* values for **c**–**h**: hypergeometric test. Results represent analyses of three biological replicates for each condition.

nature research

Corresponding author(s): Kun-Liang Guan

Reporting Summary

Nature Research wishes to improve the reproducibility of the work that we publish. This form provides structure for consistency and transparency in reporting. For further information on Nature Research policies, see Authors & Referees and the Editorial Policy Checklist.

Statistical parameters

When statistical analyses are reported, confirm that the following items are present in the relevant location (e.g. figure legend, table legend, main text, or Methods section).

n/a	Confirmed	
☐	☒	The exact sample size (*n*) for each experimental group/condition, given as a discrete number and unit of measurement
☐	☒	An indication of whether measurements were taken from distinct samples or whether the same sample was measured repeatedly
☐	☒	The statistical test(s) used AND whether they are one- or two-sided *Only common tests should be described solely by name; describe more complex techniques in the Methods section.*
☒	☐	A description of all covariates tested
☒	☐	A description of any assumptions or corrections, such as tests of normality and adjustment for multiple comparisons
☐	☒	A full description of the statistics including central tendency (e.g. means) or other basic estimates (e.g. regression coefficient) AND variation (e.g. standard deviation) or associated estimates of uncertainty (e.g. confidence intervals)
☐	☒	For null hypothesis testing, the test statistic (e.g. *F*, *t*, *r*) with confidence intervals, effect sizes, degrees of freedom and *P* value noted *Give P values as exact values whenever suitable.*
☒	☐	For Bayesian analysis, information on the choice of priors and Markov chain Monte Carlo settings
☒	☐	For hierarchical and complex designs, identification of the appropriate level for tests and full reporting of outcomes
☒	☐	Estimates of effect sizes (e.g. Cohen's *d*, Pearson's *r*), indicating how they were calculated
☐	☒	Clearly defined error bars *State explicitly what error bars represent (e.g. SD, SE, CI)*

Our web collection on statistics for biologists may be useful.

Software and code

Policy information about availability of computer code

Data collection	Igor 6.34A software for AFM data collection. NIS elements imaging software for immunofluorescence data collection.
Data analysis	The Statistical analyses were performed with Microsoft Excel for t test and Graphpad Prism 6 for two-way ANOVA test. NIS elements imaging software and Image J for immunofluorescence analyses. Igor 6.34A software for AFM data analyses.

For manuscripts utilizing custom algorithms or software that are central to the research but not yet described in published literature, software must be made available to editors/reviewers upon request. We strongly encourage code deposition in a community repository (e.g. GitHub). See the Nature Research guidelines for submitting code & software for further information.

Data

Policy information about availability of data

All manuscripts must include a data availability statement. This statement should provide the following information, where applicable:

- Accession codes, unique identifiers, or web links for publicly available datasets
- A list of figures that have associated raw data
- A description of any restrictions on data availability

Data availability. The source data for the graph representations can be found in the online version of the paper. For uncropped images of Western blot data, see

Supplementary Figure 1. The RNA sequencing data is available in GEO DataSets with the accession number GSE98547. All other data that support the findings of this study are available upon request from the corresponding author.

Field-specific reporting

Please select the best fit for your research. If you are not sure, read the appropriate sections before making your selection.

☒ Life sciences ☐ Behavioural & social sciences ☐ Ecological, evolutionary & environmental sciences

For a reference copy of the document with all sections, see nature.com/authors/policies/ReportingSummary-flat.pdf

Life sciences study design

All studies must disclose on these points even when the disclosure is negative.

Sample size	We did not use statistical method to pre-determine sample size. The sample size was based on the literature that tested the same cell lines or performed the similar assays.
Data exclusions	We did not exclude any data.
Replication	All the experiments have been at least replicated once. All the results have been validated in the repeat experiments.
Randomization	For the xenograft studies, the mice were randomly divided into different groups according to ID number.
Blinding	The investigators were blinded to group allocations during the data collection and analyses.

Reporting for specific materials, systems and methods

Materials & experimental systems

n/a	Involved in the study
☒	☐ Unique biological materials
☐	☒ Antibodies
☐	☒ Eukaryotic cell lines
☒	☐ Palaeontology
☐	☒ Animals and other organisms
☒	☐ Human research participants

Methods

n/a	Involved in the study
☒	☐ ChIP-seq
☒	☐ Flow cytometry
☒	☐ MRI-based neuroimaging

Antibodies

Antibodies used

Antibodies
Gene Usage Vendor Catalog Dilution
Actin WB Sigma A5441 1:3000
ARHGAP29 WB Santa Cruz Biotechnology sc-365554 1:400
beta-catenin IF BD Biosciences 610154 1:250
DYKDDDDK (Flag) Tag IF Cell Signaling Technology 8146 1:500
pERK1/2 WB Cell Signaling Technology 4370 1:2000
Flag WB Sigma F1804 1:2000
GAPDH WB Cell Signaling Technology 5174 1:2500
GFP IF Cell Signaling Technology 2956 1:100
GM130 IHC BD Biosciences 610823 1:500
GST WB Sigma SAB4200237 1:5000
HA IF Cell Signaling Technology 3724 1:500
HA WB Biolegend 901513 1:2000
HLA class 1 IHC Abcam ab70328 1:100
Laminin V IHC EMD Millipore MAB19562X 1:1000
LATS1 WB Cell Signaling Technology 3477 1:2000
pLATS-HM (pLATS1-T1079) Cell Signaling Technology 8654 1:2000
MST1 WB Cell Signaling Technology 3682 1:2000
MST2 WB Abcam ab52641 1:2000
PDZGEF2 WB Santa Cruz Biotechnology sc-398642 1:400
RhoA WB Cell Signaling Technology 2117 1:1000

Ras WB Cell Signaling Technology 3339 1:2000
Ras (G12V) WB Cell Signaling Technology 14412 1:2000
PLCγ1 WB Cell Signaling Technology 5690 1:1000
PLD1 WB R&D systems F5615-SP 1:1000
PLD2 WB Cell Signaling Technology 13904 1:1000
RAP2 WB BD Biosciences 610215 1:1000
TWIST IF Santa Cruz Biotechnology sc-81417 1:100
vinculin WB Sigma V9131 1:3000
YAP/TAZ IHC Cell Signaling Technology 8418 1:100
YAP/TAZ IF/WB Santa Cruz Biotechnology sc-101199 1:200 (IF) or 1:1000 (WB)
pYAP-S127 Cell Signaling Technology 4911 1:2000

Validation

Most of the antibodies are validated by Western blot or immunofluorescence with CRISPR KO cells or the cells without the expression of the antigens.

Eukaryotic cell lines

Policy information about cell lines

Cell line source(s)

HEK293A cells were provided by Ryan Russel (Univ. of Ottawa). MCF10A, MCF7, and MDA-MB-468 cells are from ATCC.

Authentication

No authentication has been used.

Mycoplasma contamination

The cells were tested for mycoplasma and they are free of mycoplasma contamination.

Commonly misidentified lines
(See ICLAC register)

None of the cells is listed in ICLAC.

Animals and other organisms

Policy information about studies involving animals; ARRIVE guidelines recommended for reporting animal research

Laboratory animals

NOD/SCID mice from JAX. 8-9 weeks old. Female.
Nude mice from UCSD. 8-9 weeks old. Female.

Wild animals

The study did not involve in wild animals.

Field-collected samples

The study did not involve in field-collected samples.